Available online at www.sciencedirect.com

ScienceDirect

Geochimica et Cosmochimica Acta 192 (2016) 1–28

Geochimica et Cosmochimica Acta

www.elsevier.com/locate/gca

Controls on the stable isotope compositions of travertine from hyperalkaline springs in Oman: Insights from clumped isotope measurements

E.S. Falk [a,*], W. Guo [a], A.N. Paukert [b,c], J.M. Matter [b,d], E.M. Mervine [a,e], P.B. Kelemen [b]

[a] *Woods Hole Oceanographic Institution, 266 Woods Hole Road, Woods Hole, MA 02543, USA*
[b] *Lamont-Doherty Earth Observatory, Columbia University, 61 Route 9W, Palisades, NY 10964, USA*
[c] *California State University Sacramento, 6000 J Street, Sacramento, CA 95819, USA*
[d] *University of Southampton, University Road, Southampton SO17 1BJ, UK*
[e] *De Beers Marine, Golf Park 2, Raapenberg Road, Pinelands, 7405 Cape Town, South Africa*

Received 14 May 2015; accepted in revised form 19 June 2016; Available online 23 June 2016

Abstract

Carbonate formation at hyperalkaline springs is typical of serpentinization in peridotite massifs worldwide. These travertines have long been known to exhibit large variations in their carbon and oxygen isotope compositions, extending from apparent equilibrium values to highly depleted values. However, the exact causes of these variations are not well constrained. We analyzed a suite of well-characterized fresh carbonate precipitates and travertines associated with hyperalkaline springs in the peridotite section of the Samail ophiolite, Sultanate of Oman, and found their clumped isotope compositions vary systematically with formation environments. Based on these findings, we identified four main processes controlling the stable isotope compositions of these carbonates. These include hydroxylation of CO_2, partial isotope equilibration of dissolved inorganic carbon, mixing between isotopically distinct carbonate end-members, and post-depositional recrystallization. Most notably, in fresh crystalline films on the surface of hyperalkaline springs and in some fresh carbonate precipitates from the bottom of hyperalkaline pools, we observed large enrichments in Δ_{47} (up to ~0.2‰ above expected equilibrium values) which accompany depletions in $\delta^{18}O$ and $\delta^{13}C$, yielding about 0.01‰ increase in Δ_{47} and 1.1‰ decrease in $\delta^{13}C$ for every 1‰ decrease in $\delta^{18}O$, relative to expected equilibrium values. This disequilibrium trend, also reflected in preserved travertines ranging in age from modern to ~40,000 years old, is interpreted to arise mainly from the isotope effects associated with the hydroxylation of CO_2 in high-pH fluids and agrees with our first-order theoretical estimation. In addition, in some fresh carbonate precipitates from the bottom of hyperalkaline pools and in subsamples of one preserved travertine terrace, we observed additional enrichments in Δ_{47} at intermediate $\delta^{13}C$ and $\delta^{18}O$, consistent with mixing between isotopically distinct carbonate end-members. Our results suggest that carbonate clumped isotope analysis can be a valuable tool for identifying and distinguishing processes not readily apparent from the carbonate bulk stable isotope compositions alone, e.g., kinetic effects or mixing of different carbonate end-members, which can significantly alter both the apparent formation temperatures and apparent radiocarbon ages. The isotope trends observed in these travertine samples could be applied more broadly to identify extinct

* Corresponding author at: North Carolina State University, 2800 Faucette Drive, Raleigh, NC 27695, USA.
E-mail address: esfalk@nscu.edu (E.S. Falk).

http://dx.doi.org/10.1016/j.gca.2016.06.026

hyperalkaline springs in terrestrial and extraterrestrial environments, to better constrain the formation conditions and post-depositional alteration of hyperalkaline spring carbonates, and to extract potential paleoclimate information.

Keywords: Clumped isotopes; Kinetic isotope fractionation; Alkaline springs; Travertine; Carbonate

1. INTRODUCTION

1.1. Carbonate formation in peridotite-hosted hyperalkaline springs

Springs emanating from serpentinized peridotite in the Samail ophiolite, Sultanate of Oman, are characterized by high pH (~11–12), high Ca^{2+} concentrations, and almost no dissolved inorganic carbon (DIC). These hyperalkaline springs react with atmospheric CO_2, resulting in rapid precipitation of calcium carbonate and formation of extensive travertine terraces (Neal and Stanger, 1985; Clark and Fontes, 1990; Kelemen and Matter, 2008; Matter and Kelemen, 2009; Kelemen et al., 2011; Paukert et al., 2012; Chavagnac et al., 2013a,b; Mervine et al., 2014, 2015).

The development of these Ca^{2+}-OH^- rich waters is typical of serpentinization in peridotite massifs worldwide (e.g., Barnes et al., 1967, 1978; Barnes and O'Neil, 1969; Neal and Stanger, 1985; Bruni et al., 2002; Neal and Shand, 2002; Marques et al., 2008; Szponar et al., 2013; Cardace et al., 2015). Such ultramafic systems have been the subject of diverse studies, with much interest in fate of carbon in these environments. The rapid uptake of CO_2 during natural carbonation of peridotite, estimated to currently be $\sim 10^3$ tons of CO_2 km^{-3} yr^{-1} in Oman, has been viewed as a promising analog for mineral carbon sequestration (e.g., Cipolli et al., 2004; Kelemen and Matter, 2008; Wilson et al., 2009). The development of hyperalkaline fluids during serpentinization has also been suggested as possible driver of carbonate precipitation and methane generation on Mars (e.g., Niles et al., 2005; Oze and Sharma, 2005; Ehlmann et al., 2010; Etiope et al., 2013; Niles et al., 2013), attracting attention to terrestrial hyperalkaline springs as potential Martian analogs (e.g., Szponar et al., 2013). In addition, there have been attempts to reconstruct paleoclimate in Oman (e.g. periods of aridity or humidity) based on variations in travertine morphology and the bulk stable isotope compositions of carbonates (Clark and Fontes, 1990).

Unlike typical travertines precipitated by degassing of CO_2 from calcium- and bicarbonate-rich waters of hydrothermal origin, which may record apparent equilibrium oxygen and clumped isotope compositions near spring vents (e.g., Kele et al., 2015), the isotope compositions of travertines formed at hyperalkaline springs usually deviate significantly from expected equilibrium values. Previous studies of peridotite-hosted travertines in Oman revealed positive correlations between their $\delta^{13}C$ and $\delta^{18}O$ values, with $\delta^{13}C$ vs. $\delta^{18}O$ slope of ~1.3 (Clark and Fontes, 1990; Clark et al., 1992; Kelemen et al., 2011; Mervine et al., 2014). The youngest travertines are often characterized by large depletions in ^{13}C and ^{18}O (Clark et al., 1992; Kelemen et al., 2011; Mervine et al., 2014), while preserved travertines generally exhibit relatively higher $\delta^{13}C$ and $\delta^{18}O$ values that may extend to values consistent with expected equilibrium with observed spring-water $\delta^{18}O$ and temperatures and atmospheric $\delta^{13}C$ (Neal and Stanger, 1985; Clark et al., 1992; Matter, 2005). Similar correlated depletions in $\delta^{13}C$ and $\delta^{18}O$ have been observed worldwide in other carbonates precipitated during interaction between alkaline waters and atmospheric CO_2. For example, the $\delta^{13}C$ and $\delta^{18}O$ values of fresh carbonate precipitates and travertines from hyperalkaline springs in northern California overlap significantly with values observed in Oman (O'Neil and Barnes, 1971; Kelemen et al., 2011). These depletions in $\delta^{13}C$ and $\delta^{18}O$ have typically been interpreted as a kinetic isotope effect resulting from CO_2 uptake from the atmosphere (O'Neil and Barnes, 1971; Clark et al., 1992; Wilson et al., 2010). In some cases depleted isotopic signatures in carbonates precipitated in alkaline environments may also be derived from nearby carbonate sediments, as was initially suggested for surface calcium carbonates associated with weathering of chrysotile tailings in northern British Columbia (Wilson et al., 2009).

1.2. Carbonate clumped isotope geochemistry

The carbonate clumped isotope thermometer is a relatively new paleothermometer based on the tendency of ^{13}C and ^{18}O isotopes to preferentially bond to one another (or "clump") within the CO_3^{2-} groups under thermodynamic equilibrium. This property is commonly measured as 'Δ_{47},' the excess of mass-47 isotopologue (primarily $^{13}C^{18}O^{16}O$) in the CO_2 evolved from phosphoric acid digestion of solid carbonate relative to the abundances expected for a stochastic distribution of all isotopes (Ghosh et al., 2006; Eiler, 2007, 2011; Huntington et al., 2009):

$$\Delta_{47} = \left[\left(\frac{R_{47}}{R^*_{47}} - 1\right) - \left(\frac{R_{46}}{R^*_{46}} - 1\right) - \left(\frac{R_{45}}{R^*_{45}} - 1\right)\right] \times 1000 \quad (1a)$$

where R_i is the measured ratio of the isotopologue of mass i and R_i^* is the ratio for a stochastic distribution. i.e.,

$$\Delta_{47} = \left[\frac{R_{47}}{2R_{13} \times R_{18} + 2R_{17} \times R_{18} + R_{13} \times (R_{17})^2} - \frac{R_{46}}{2R_{18} + 2R_{13} \times R_{17} + (R_{17})^2} - \frac{R_{45}}{R_{13} + 2R_{17}} + 1\right] \times 1000 \quad (1b)$$

Unlike conventional carbonate-water oxygen isotope thermometry, the extent of this clumping effect, under thermodynamic equilibrium, depends only on the equilibration temperature and not on the isotopic composition of the

waters from which the carbonate precipitated. This makes it a valuable tool for a variety of applications, especially in cases where the isotopic composition of the parent waters are difficult to constrain, e.g. paleoclimate, paleoaltimetry, diagenesis, and low grade metamorphism (see reviews in Eiler, 2011; Affek, 2012; Huntington and Lechler, 2015).

Although inter-laboratory differences remain in the calibration of the carbonate clumped isotope paleothermometer, calibrations among a variety of natural and synthetic carbonates have so far yielded remarkably consistent results within individual laboratories considering the range of materials studied (e.g., Ghosh et al., 2006; Dennis and Schrag, 2010; Tripati et al., 2010; Eiler, 2011; Eagle et al., 2013; Grauel et al., 2013; Henkes et al., 2013; Zaarur et al., 2013; Defliese et al., 2015; Kele et al., 2015; Kluge et al., 2015). Mostly notably, the clumped isotope compositions of some carbonate materials that were known to be affected by kinetic effects in bulk stable isotopes, such as certain deep-sea corals, foraminifera and coccoliths, appear to conform to the equilibrium temperature calibration relationship derived from inorganic carbonates precipitated in the laboratory (e.g., Tripati et al., 2010; Thiagarajan et al., 2011). However, there is increasing evidence that disequilibrium clumped isotope effects also exist in nature, especially for several types of carbonates, e.g. speleothems, cryogenic carbonates (e.g., Affek et al., 2008, 2014; Guo, 2008; Daeron et al., 2011; Wainer et al., 2011; Kluge and Affek, 2012; Kluge et al., 2014), some shallow-water and cold-water corals (Saenger et al., 2012; Spooner et al., 2016). These disequilibrium clumped isotope effects, if not corrected for, would lead to systematic over-estimation (e.g. for speleothems and cryogenic carbonates) or under-estimation (e.g. for some corals) of the carbonate formation temperatures derived from the clumped isotope thermometer. Our current understanding of the causes of these disequilibrium effects is still limited, but most of these effects are thought to be related to the kinetic isotope fractionations associated with the CO_2 hydration/hydroxylation reactions and their reverse reactions (e.g., Guo, 2008; Saenger et al., 2012; Affek et al., 2014; Spooner et al., 2016). The same reactions, particularly CO_2 hydroxylation, play key roles in carbonate formation during rapid uptake of CO_2 at alkaline springs, as in Oman (Clark et al., 1992). Here we present an investigation of the clumped isotope systematics of carbonates formed in hyperalkaline springs in Oman, and discuss the implication of our findings for the interpretation of the isotopic compositions of travertines formed in similar environments.

2. GEOLOGIC SETTING AND TRAVERTINE FORMATION IN OMAN

The Samail ophiolite, in the Sultanate of Oman and the United Arab Emirates (Fig. 1), represents one of the largest exposures of mantle peridotite on land. The mantle peridotite section is composed of residual harzburgites and dunites and is variably serpentinized, typically ~30–80% (e.g., Boudier and Coleman, 1981; Godard et al., 2000; Monnier et al., 2006; Hanghøj et al., 2010), with completely serpentinized peridotite commonly observed in more altered sections. Much of this serpentine is thought to have formed during suboceanic hydrothermal alteration prior to exposure of the ophiolite on land (e.g., Boudier et al., 2010), but low temperature serpentinization continues today during reaction of meteoric water with peridotite (e.g., Barnes and O'Neil, 1969; Neal and Stanger, 1983; Streit et al., 2012).

This ongoing low temperature alteration of peridotite leads to the formation of hyperalkaline springs and abundant carbonate precipitation via three steps. (1) Meteoric surface waters react with shallow peridotite in an open system that remains in equilibrium with atmospheric CO_2 and O_2. This results in the formation of waters rich in Mg^{2+}-HCO_3^-, also known as "Type I" waters (Barnes and O'Neil, 1969). (2) As surface waters percolate deeper into the peridotite, they become isolated from the atmosphere. The formation of Mg-rich alteration products, such as serpentine and Mg-carbonate, in this subsurface environment leads to decreases in concentrations of Mg^{2+} and DIC, while Ca^{2+} continues to accumulate in the groundwater through continued dissolution of peridotite. This results in the formation of alkaline Ca^{2+}-OH^- waters, also known as "Type II" waters, characterized by high pH (up to 12), low Eh (approximately −200 mV), and virtually no Mg^{2+} (typically $<10^{-2}$ mmol/L) or DIC (typically $\sim10^{-1}$ mmol/L) (Barnes and O'Neil, 1969; Neal and Stanger, 1985; Bruni et al., 2002; Paukert et al., 2012; Chavagnac et al., 2013b). (3) When these Ca^{2+}-OH^- waters reach the surface as hyperalkaline springs, rapid precipitation of calcium carbonate results from reaction with CO_2, either by direct uptake of atmospheric CO_2 or mixing with shallow groundwater or surface waters containing ~3–5 mmol/L DIC (Paukert et al., 2012).

Alkaline springs of this type are common throughout the peridotite section of the Samail ophiolite, with close to 100 such springs identified in previous studies (e.g., Neal and Stanger, 1985; Kelemen and Matter, 2008; Paukert et al., 2012; Chavagnac et al., 2013b). Where alkaline spring water comes in contact with atmospheric CO_2, crystalline films of calcium carbonate may form on the surface of pools. This reaction is rapid enough that calcium carbonate crusts ~0.5 mm thick re-form on the surface of the pools within a couple days when they are removed by rainstorms or manually. In many locations, these alkaline springs form a series of striking, milky-blue pools lined with white unconsolidated calcium carbonate precipitates, particularly where springs emerge along wadi (stream) beds. Alkaline spring water may also flow along the surface of travertine terraces in shallow trickles without the development of larger pools or may form speleothem-like carbonate structures where eroded peridotite outcrops form overhangs that allow alkaline water to drip freely. In previous studies of carbonate mineralogy at alkaline springs, fresh calcium carbonate precipitates have been found to be mixtures of calcite and aragonite, with calcite more common in surface films and aragonite more common in bottom deposits (Paukert et al., 2012; Chavagnac et al., 2013a; Mervine et al., 2014).

Over time, calcium carbonate precipitation associated with these hyperalkaline springs has resulted in the

Fig. 1. Location of hyperalkaline springs and associated travertine terraces where fresh carbonate precipitates and preserved travertines were sampled in this study (black dots). Samail ophiolite shown in green. (For interpretation of the references to colour in this figure legend, the reader is referred to the web version of this article.)

build-up of extensive travertine terraces, typically ~200,000 m^2 in area and ~1 m thick, in areas surrounding active springs (Kelemen and Matter, 2008). Radiometric dating and measurements of layer thickness within travertine terraces suggests that travertine deposition has been ongoing for at least 50,000 years, with average deposition rates of ~0.1–0.3 mm/year (Kelemen and Matter, 2008; Mervine et al., 2014). Clark and Fontes (1990) had previously argued that surficial travertine deposits in Oman were only deposited and preserved during periods of hyperaridity, but subsequent studies have identified travertine terraces with ^{14}C ages that fill in the gaps in the Clark and Fontes (1990) record (Kelemen and Matter, 2008; Mervine et al., 2014).

3. MATERIAL AND METHODS

3.1. Description of carbonate samples

A total of 29 samples of fresh carbonate precipitates from alkaline springs and 14 preserved travertines were collected from 9 locations throughout the southern portion of the Samail ophiolite (Fig. 1) over several field seasons, each January between 2007 and 2012. Sample locations and descriptions are presented in Table 1, and photos of some sampling locations are shown in Fig. 2. Many of these samples (10 fresh carbonate precipitates and 14 travertines, as indicated in Table 1) have been included in previous studies of hyperalkaline springs and travertine formation in Oman, in which their mineralogical composition, carbon and oxygen isotope composition, and/or ^{14}C ages were reported (Kelemen et al., 2011; Paukert et al., 2012; Falk, 2013; Mervine et al., 2014). None of the samples have been analyzed before for their clumped isotope compositions. In this study, we performed clumped isotope analysis on 28 of these carbonate samples and only bulk carbon and oxygen isotope analysis on the other 15 samples.

The fresh carbonate precipitates we collected from hyperalkaline springs can be grouped into two main types: (1) "surface films"—thin crystalline films or crusts formed at the surface of hyperalkaline springs (e.g., Fig. 2C)—and (2) "bottom floc"—the unconsolidated carbonate lining hyperalkaline spring pools and outlet channels. Bottom floc samples can be further divided based on their depositional environments. Some are found in larger hyperalkaline spring pools within wadi (stream) beds (e.g., Fig. 2A), while others form in smaller pools and thin flows along the surface of travertine terraces (e.g., Fig. 2B and D). All surface films were collected directly at the hyperalkaline spring source. Bottom floc samples were collected either directly at the hyperalkaline spring source or at downstream locations close enough to the spring that water pH remained above 11. Carbonates collected at the exact same location as water samples are listed with their corresponding water samples in Table 2. These include "flow path" samples—samples collected downstream from the alkaline spring outlet, with distance from the spring indicated in Table 2.

The travertine samples in this study include recently-formed travertine layers from areas of active travertine

Table 1
Surface carbonate samples associated with alkaline springs.

Sample	Location	Type	UTM-E[a]	UTM-N[a]	^{14}C Age[b]	Refs.[c]	Major carb min[d]	Minor carb min[e]	Refs.[f]
Fresh precipitates from alkaline springs – samples with clumped isotopes analyzed at WHOI									
OM10-6COPS	Al Bana	Bottom floc, man-made	487316	2576132	>Modern	4	Calcite	Aragonite	4
OM12_07V	Al Bana	Bottom floc, shallow flow	489560	2575440			Calcite + aragonite		This study
OM12_07X2	Al Bana	Bottom floc, pool	489560	2575440			Calcite + aragonite		This study
OM12_09AA	Al Hilayw	Bottom floc, shallow flow	585880	2523240			Calcite, aragonite		This study
OM12_09AE	Al Hilayw	Bottom floc, shallow pool	585880	2523240			Calcite + aragonite		This study
OM11_07U	Misbit	Bottom floc, pool	625990	2576260			Calcite, aragonite		2
OM11_07V	Misbit	Surface film, pool	625990	2576260			Calcite, aragonite		2
OM11_07Y	Misbit	Bottom floc, wadi mixing	625990	2576260			Aragonite, calcite		2
OM09-6COPS	Qafeefah	Bottom floc, pool	646107	2533645	295	4	Aragonite	Calcite	4
OM09-7COPS	Qafeefah	Bottom floc, pool	646107	2533645	350	4	Aragonite	Calcite	4
OM10-1COPS	Qafeefah	Surface film	646117	2533648	>Modern	4	Calcite		4
OM10-2COPS	Qafeefah	Bottom floc, pool	646072	2533678	>Modern	4	Aragonite	Calcite	4
OM09-8COPS	Wadi Sudari	Bottom floc, pool	443118	2650078	>Modern	4	Calcite, aragonite		4
OM09-10COPS	Wadi Uqaybah	Surface film	426183	2633965	>Modern	4	Calcite		4
Fresh precipitates from alkaline spring flow paths – samples with only $\delta^{13}C$ and $\delta^{18}O$ analyzed at University of Waterloo									
OM12_07U	Al Bana	Bottom floc	489560	2575440					
OM12_07W1	Al Bana	Surface film	489560	2575440					
OM12_07W2	Al Bana	Bottom floc	489560	2575440					
OM12_07X1	Al Bana	Surface film	489560	2575440					
OM12_01A	Falaij	Bottom floc	608440	2525960					
OM12_01B	Falaij	Bottom floc	608440	2525960					
OM12_01C1	Falaij	Surface film	608440	2525960					
OM12_01C2	Falaij	Bottom floc	608440	2525960					
OM12_01D	Falaij	Bottom floc	608440	2525960					
OM12_01E1	Falaij	Bottom floc	608440	2525960					
OM12_01E2	Falaij	Surface film	608440	2525960					
OM12_01F1	Falaij	Surface film	608440	2525960					
OM12_01F2	Falaij	Bottom floc	608440	2525960					
OM12_01G1	Falaij	Surface film	608440	2525960					
OM12_01G2	Falaij	Bottom floc	608440	2525960					
Travertine deposits									
OM08-200	Kharma	Recent travertine	600173	2528469	305	1	Calcite		3
OM07-34c	Wadi Mahram	Recent travertine	608365	2526870	>Modern	1	Calcite		3
OM09-85C-MS	Wadi Sudari	Recent travertine	443082	2650304	>Modern	4	Calcite		4
OM09-89C-MS	Wadi Sudari	Recent travertine	443118	2650078	>Modern	4	Calcite	Aragonite	4
OM10-32C-1	Al Bana	Travertine terrace	487305	2576134	44700	4	Calcite		4
OM10-32C-2	Al Bana	Travertine terrace	487305	2576134	42500	4	Calcite		4
OM10-32C-6	Al Bana	Travertine terrace	487305	2576134	34040	4	Calcite	Dolomite	4
OM10-32C-8	Al Bana	Travertine terrace	487305	2576134	18350	This study	Calcite		4
OM10-32C-9	Al Bana	Travertine terrace	487305	2576134	32010	4	Calcite		4

OM10-32C-10	Al Bana	Travertine terrace	487305	2576134	15640	This study	Calcite		4
OM10-32C-11	Al Bana	Travertine terrace	487305	2576134	8890	4	Calcite		4
OM10-78C-3	Wadi Uqaybah	Travertine terrace	426266	2633919	41610	4	Calcite		4
OM10-78C-4	Wadi Uqaybah	Travertine terrace	426266	2633919	39530	4	Calcite	Dolomite	4
OM10-78C-6	Wadi Uqaybah	Travertine terrace	426266	2633919	37540	4	Calcite		4

[a] UTM coordinates in Zone 40Q. Coordinates where both easting and northing end in zero are approximate, estimated to nearest 10 m.
[b] Calibrated ^{14}C age, years before present. By convention, "present" = 1950.
[c] References for ^{14}C ages: 1 – Kelemen et al., 2011; 2 – Paukert et al., 2012; 3 – Falk, 2013; 4 – Mervine et al., 2014.
[d] Major carbonate minerals (>approx 20%), more abundant mineral listed first; Calcite + aragonite indicates roughly equal proportions.
[e] Minor carbonate minerals (<approx 10%).
[f] References for mineralogy: 1 – Kelemen et al., 2011; 2 – Paukert et al., 2012; 3 – Falk, 2013; 4 – Mervine et al., 2014.

deposition and older laminated travertine terraces (Fig. 2F). Specifically, the older travertine samples consist of carefully subsampled layers of a ~2 m thick travertine section from Al Bana (i.e., the Misht Travertine location; Mervine et al., 2014) and a ~1 m thick travertine section from the Wadi Uqaybah travertine, both of which were previously described and radiocarbon dated by Mervine et al. (2014). There are no active hyperalkaline springs flowing along the surfaces of these older travertines where these samples were collected, but they are located in the general vicinity of active hyperalkaline springs.

Sample collection and processing methods for fresh precipitates, preserved travertines, and associated water samples are described in detail by Paukert et al. (2012) and Mervine et al. (2014). Briefly, fresh precipitates collected from hyperalkaline pools were allowed to dry at ambient conditions and later dried in a 40 °C oven. Because of the very fine-grained nature of these precipitates, crushing and mechanical powdering of these samples was not necessary prior to mineralogical and isotopic analyses. Preserved travertine rock samples collected in 2007–2009 were crushed in a jaw crusher and powdered in a puck mill or with an agate mortar and pestle. Layers from travertines collected in 2010 were carefully subsampled at millimeter scales using a micromill, as previously described in Mervine et al. (2014).

3.2. Properties of spring water

In situ and laboratory-based measurements were made on spring water from hyperalkaline pools and flow paths along the surface of travertine terraces, to determine water temperature, pH, major element chemistry and stable isotopic compositions (Table 2). These field data and water samples were obtained in 2008–2012 (year of collection indicated by sample prefix), during the same field seasons as the carbonate samples described above, and several pools ("sites") were re-visited over the course of multiple field seasons. Many of the fresh carbonate samples discussed in this study were collected from the same pools as the spring water samples, as indicated in Table 2. In most of those cases, collection of water samples and in situ measurements of pH were made at the time of collection of fresh carbonate precipitates. Additional data for some of the water samples (e.g., conductivity, oxidation–reduction potential, and major and trace element concentrations) have been reported previously in Paukert et al. (2012), as indicated in Table 2.

In situ measurements of the pH and temperature of alkaline springs were conducted using a WTW Multi 3400i multi-parameter field meter (Paukert et al., 2012). Major cation compositions were determined by inductively coupled plasma atomic emission spectrometry (ICP-AES) on a Horiba Jobin-Yvon Activa M spectrometer at Columbia University, by inductively coupled plasma atomic absorption spectrometry on a Perkin-Elmer AAnalyst 800 spectrometer at CUNY Queens College, and an inductively coupled plasma mass spectrometer at Arizona State University. DIC concentrations were measured at Arizona State University on an OI Analytical Model 1010 Wet Oxidation TOC Analyzer for samples from the 2009

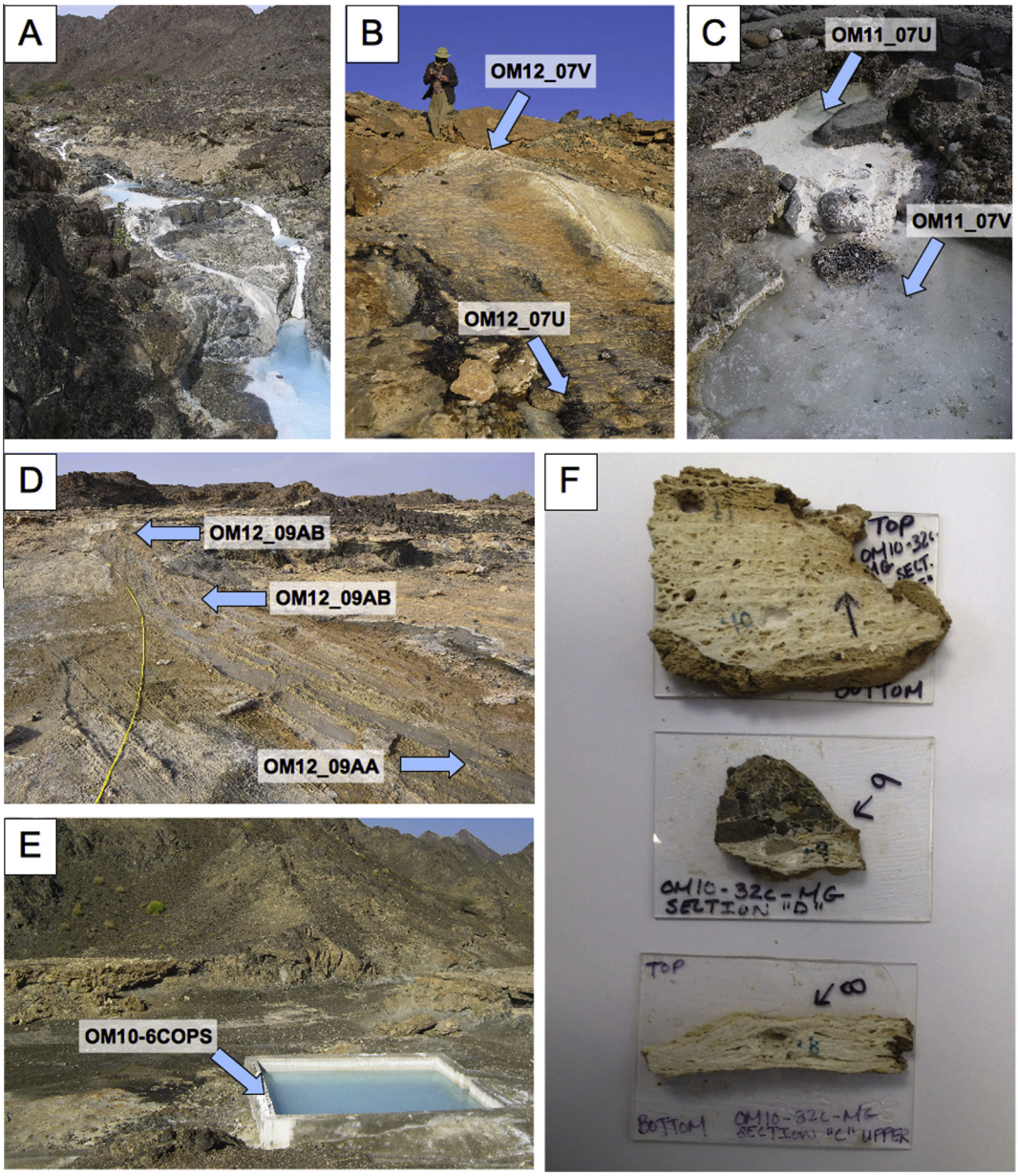

Fig. 2. Photographs of hyperalkaline spring sampling sites and subsampled travertine terraces. (A) Hyperalkaline blue pools within streambed at Qafeefah. (B) Shallow flow of hyperalkaline fluids along the surface of travertine terraces at Al Bana, flow path sampling of carbonate and spring water at OM12_07V and OM12_07U. (C) Surface film (OM11_07V) and bottom floc (OM11_07U) from Misbit Spring pool. (D) Shallow flow of hyperalkaline fluids along the surface of travertine terraces at Al Hilayw, flow path sampling of spring water at OM12_09AA, OM12_09AB, OM12_09AC and sampling of fresh precipitates (bottom floc) at OM12_09AA. (E) Man-made elevated pool collecting alkaline spring water (OM10-6COPS) at Al Bana travertines. (F) Subsampled travertine terrace from Wadi Uqaybah (OM10-32C subsamples 8, 9, 10, 11). (For interpretation of the references to colour in this figure legend, the reader is referred to the web version of this article.)

and 2010 field season and at Columbia University via acidification on a UIC CM5230 carbon analyzer for samples from the 2012 field season. The analytical precisions were ±2% and ±1% (relative standard deviation) for major cation concentrations and DIC concentration measurements, respectively.

$\delta^{18}O$ and δD of water, and $\delta^{13}C$ of DIC were measured by isotope ratio mass spectrometry (IRMS) in the Environmental Isotopes Laboratory at the University of Waterloo. $\delta^{18}O$ of water was determined by the CO_2 equilibration method (Epstein and Mayeda, 1953), using a VG 903 mass spectrometer for samples from the 2008 field season (prefix "OM08-") and using a Micromass IsoPrime mass spectrometer for all other samples. δD of water was analyzed by the chromium reduction method on a Eurovector Euro 3000 Elemental Analyzer coupled to a Micromass IsoPrime mass spectrometer (Gehre et al., 1996). For carbon isotope measurements of DIC, water was reacted

under vacuum with anhydrous (100%) H_3PO_4 (McCrea, 1950), and the liberated CO_2 was then directly released into a Micromass IsoPrime mass spectrometer via a Gilson 222XL auto-sampler. The overall analytical precisions were ±0.2‰, ±0.8‰, and ±0.2‰ (1 S. D.) for $\delta^{18}O_{water}$, δD, and $\delta^{13}C_{DIC}$, respectively. The isotopic data are reported relative to Vienna Standard Mean Ocean Water (VSMOW) and Vienna Pee-Dee Belemnite (VPDB).

3.3. Carbonate mineral identification

For fresh carbonate precipitates collected in 2012 that were subject to clumped isotope analysis, calcium carbonate minerals were identified by Raman spectroscopy using a Horiba LabRAM HR confocal Raman spectrometer at Woods Hole Oceanographic Institution (WHOI). Spectra were collected for 5 s with 3 accumulations averaged for each analysis spot. Each sample was analyzed at four spots and each spectrum was classified as calcite, aragonite, or a very fine-grained mixture of both in order to reflect the relative proportions of each mineral.

The mineralogy of samples collected in 2007–2011 was determined by powder X-ray diffraction (XRD) and reported in detail in previous studies (Kelemen et al., 2011; Paukert et al., 2012; Falk, 2013; and Mervine et al., 2014). Semi-quantitative estimates of mineral proportions based on relative peak intensities of X-ray diffraction spectra were used to classify each mineral as major (>∼20%) or minor (<∼10%) in these samples, as reported in Table 1.

3.4. Radiocarbon dating of travertines

All ^{14}C ages of preserved travertines were determined at the National Ocean Sciences Accelerator Mass Spectrometry Facility (NOSAMS) at Woods Hole Oceanographic Institution, including data reported in previous studies and new ages obtained for this study. Most of the ^{14}C ages reported in Table 1 were obtained by Mervine et al. (2014), and detailed methods are reported in that publication. Additional ^{14}C ages were obtained on recent travertine samples OM07-34C and OM08-200 in 2008 and reported in Kelemen et al. (2011). Two travertine terrace subsamples previously analyzed by Mervine et al. (2014), OM10-32C-8 and OM10-32C-10, were submitted to NOSAMS for re-analysis in 2014, and these new data are reported in Table 1. All ^{14}C data were corrected for isotopic fractionation using $\delta^{13}C$ values measured on the accelerator. ^{14}C ages were calculated using 5568 years as the half-life and converted to calibrated ages using the Calib 7.1 Program with the IntCal13 calibration curve (Reimer et al., 2013). Because alkaline spring water emerges with essentially no dissolved carbon and most carbonates form from direct uptake of atmospheric CO_2, no correction for the possible effects of dead carbon is made in the calculation of ^{14}C ages (Mervine et al., 2014).

3.5. Stable isotope measurements of carbonates

3.5.1. Carbon and oxygen isotope measurement

Stable carbon and oxygen isotope compositions were determined for all carbonate samples. $\delta^{13}C$ and $\delta^{18}O$ data for fresh carbonate precipitates collected along alkaline spring flow paths at Falaij and Al Bana travertine sites in 2012 were obtained in the Environmental Isotopes Laboratory at the University of Waterloo using a GVI IsoPrime continuous flow isotope ratio mass spectrometer system (CF-IRMS) following automated phosphoric acid digestion at 90 °C. The external precisions for these measurements are ±0.2‰ (1 S.D.) for $\delta^{18}O$ and ±0.1‰ (1 S.D.) for $\delta^{13}C$. Bulk stable isotopic data ($\delta^{13}C$ and $\delta^{18}O$) for two of these samples and all other carbonate samples were obtained at Woods Hole Oceanographic Institution simultaneously with Δ_{47}, as part of the clumped isotope measurement, and were normalized by reference to the carbonate standard NBS-19 analyzed in each analytical session, with precisions of ±0.08‰ and ±0.10‰ (1 S.D.) respectively. All the carbonate isotope values are reported relative to Vienna Pee-Dee Belemnite (VPDB) in Table 3.

3.5.2. Clumped isotope measurement: Method

Clumped isotope analyses were performed at Woods Hole Oceanographic Institution on a Thermo MAT-253 stable isotope mass spectrometer coupled to an automated sample digestion and purification line (Thornalley et al., 2015; Spooner et al., 2016). For each carbonate measurement, 3–5 mg of powdered sample material are loaded into silver capsules for in vacuo digestion in a common acid bath of 103% phosphoric acid ($\rho = 1.92$ g/cm^3) at 90 °C for 20 min. During this reaction, evolved CO_2 is continuously frozen into a trap immersed in a dewar of liquid nitrogen (LN2), after passing through a cryogenic trap maintained at −78 °C. Upon completion of the acid digestion step, the collection trap is warmed to −78 °C, and the CO_2 is transported by a He carrier gas at a controlled flow rate of 30 ml/minute through a custom-made 60 cm long gas chromatography (GC) column (Porapak Q, 50–80 mesh) held at −20 °C before being collected in a second LN2 trap. After the He carrier gas is pumped away, the purified CO_2 is again warmed to −78 °C and transferred to a small glass LN2 trap. The CO_2 is then allowed to expand into the sample bellow of the mass spectrometer. All gas standards (i.e. heated gases and equilibrated gases; see Section 3.5.3) used in the construction of the absolute reference frame are introduced and purified in the same manner as CO_2 derived from carbonate samples: passing through a −78 °C trap and allowed to collect in a LN2 trap for 20 min before further GC and cryogenic purification. Purified CO_2 were measured against a bottle of working reference CO_2 (Oztech CO_2, $\delta^{18}O_{VSMOW} = 25.04$‰, $\delta^{13}C_{VPDB} = -3.63$ ‰) at a bellow pressure resulting in a signal of 12 V on mass-44. Each clumped isotope measurement consists of 6 acquisitions, with 9 cycles of sample-reference comparison (20 s of integration time) in each acquisition.

3.5.3. Clumped isotope measurement: Data reduction

Carbonate samples were analyzed over the course of three analytical sessions (January–February, March–April, and July 2014), with each sample analyzed 3–8 times. Four measurements from the first analytical session were excluded from the final sample averages because $\delta^{13}C$ and $\delta^{18}O$ values were several permil higher than other replicate

Table 2
Water data from alkaline springs.

Sample ID[a]	Location	Site[b]	Dist., m[c]	pH	T °C	$\delta^{18}O$, ‰ VSMOW	$\delta^{2}H$, ‰ VSMOW	$\delta^{13}C_{DIC}$, ‰ VPDB	DIC, mmol/L[d]	Ca, mmol/L[d]	Mg, mmol/L[d]	Paukert[e]	Carbonate samples[f]
OM10_05AA	Al Bana	Aardvark		11.65	28.5	0.09	−0.85	−19.71	0.26	1.66	3.0E−02	√	
OM10_06AH	Al Bana	Al Ohwenah		11.16	38.4	−1.08	−4.08	−19.42	0.16	2.01	1.8E−02	√	
OM10_06AG	Al Bana	Al Thurawah		11.14	37.7	−0.42	−2.40	−17.82	0.18	1.54	9.4E−03	√	
OM09_W14H	Al Bana	Fork		12.08	26	0.54	−1.04	−11.66	0.20				
OM09_W14I	Al Bana	Gas Crack		11.84	32	1.89	−1.79	−13.24	0.22				
OM10_05AD	Al Bana	Gas Crack		11.68	32.6	1.15	−2.59	−14.8	0.22	2.11	3.3E−02	√	
OM10_05AF	Al Bana	Spine Mama		11.9	24.2	0.51	0.38	−23.67	0.26	1.57	2.7E−02	√	OM12_07X1,2
OM12_07X	Al Bana	Spine Mama	0	11.60	28.3	−0.62	−3.23	NA	0.12	1.60	BDL		OM12_07X1*,2**
OM12_07W	Al Bana	Papa	2.9	11.63	28.7	−0.61	−3.25	NA		1.83	BDL		OM12_07W1*,2*
OM12_07V	Al Bana	Sister	5.3	11.58	28.7	−0.63	−3.36	−18.36		1.78	BDL		OM12_07V**
OM12_07U	Al Bana	Brother	12.8	11.39	28.0	0.95	3.48	−26.82		0.57	BDL		OM12_07U*
OM08_W09	Al Hilayw			11.28		0.75	6.91						
OM08_W10	Al Hilayw			11.31		0.62	5.98						
OM08_W11	Al Hilayw			11.32		1.00	3.28						
OM08_W12	Al Hilayw			11.32		0.51	4.22						
OM08_W13	Al Hilayw			11.35		−0.21	1.08						
OM12_09AE	Al Hilayw	Land Cruiser	0	11.39	25.9	0.50	3.94	NA		1.49	BDL		OM12_09AE**
OM12_09AD	Al Hilayw	Camel	2.3	11.40	25.8	0.57	4.49	−24.11		1.51	BDL		
OM12_09AC	Al Hilayw	Sandal	6.8	11.41	24.8	0.64	4.82	−23.95		1.42	BDL		
OM12_09AB	Al Hilayw	Bedu Truck	12	11.43	24.1	1.00	6.38	NA		1.17	BDL		
OM12_09AA	Al Hilayw	Moped	17	11.31	22.5	1.63	9.24	−18.35		0.82	BDL		OM12_09AA**
OM09_W04F	Al Hilayw	Lungs		11.76	25.6	1.74	5.64	NA	0.22	1.40	8.6E−03	√	
OM09_W04G	Al Hilayw	Jimi		11.77	27.1	2.02	6.02	−28.73	0.02	1.31	9.1E−03	√	
OM09_W04H	Al Hilayw	Africa		11.51	24.5	2.50	9.75		0.78				
OM09_W04I	Al Hilayw	dnstr of Jimi		11.9	20.7	1.98	7.82	−21.38	0.20	1.07	9.7E−03	√	
OM08_W01	Bahla			11.49		0.59	4.91						
OM08_W 17	Dima			11.2		−0.18	0.30						
OM09_W06O	Dima	Pacman		11.54	30.3	0.52	−0.14	−12.99	0.16	1.82	7.2E−03	√	
OM08_W02	Falaij			10.5		−0.40	−0.55						
OM08_W03	Falaij			11.38		−0.35	0.53						
OM08_W04	Falaij			11.15		−0.29	−0.47						
OM08_W05	Falaij			11.38		−0.36	1.41						
OM09_W02A	Falaij 1	Falaij Spring		11.52	29.1	0.74	1.96	NA	0.18				
OM10_02L	Falaij 1	Falaij Spring		11.52	30.8	0.65	0.85	−17.42	0.20	1.83	2.5E−02	√	
OM12_01G	Falaij 1	Falaij Spring	0	11.25	30.3	−0.53	−1.16	−17.46	0.11	2.03	1.3E−02		OM12_01G1*,2*
OM12_01F	Falaij 1	Ogre	5.5	11.22		−0.48	−1.09	−16.07	0.09	2.07	BDL		OM12_01F1*,2*
OM12_01E	Falaij 1	Hobbit	11.5	11.35		−0.49	−1.14	−17.83	0.09	2.09	BDL		OM12_01E1*,2*
OM12_01D	Falaij 1	Elf	14.7	11.31		−0.51	−1.21	−18.71	0.10	2.11	BDL		OM12_01D*
OM12_01C	Falaij 1	Angry Worm	16.6	11.28		−0.48	−1.46	−18.00	0.11	2.10	BDL		OM12_01C1*,2*
OM12_01B	Falaij 1	Dwarf	19.5	11.25		−0.45	−0.93	−18.57	0.12	2.11	BDL		OM12_01B*
OM12_01A	Falaij 1	Little Knobby	24.5	11.24		−0.45	−1.02	−18.88	0.14	2.09	BDL		OM12_01A*

OM10_03R	Falaij 2	Little Mermaid		11.63	27.9	1.12	6.33	−16.78	0.16	1.67	3.7E−02	√	
OM12_02L	Falaij 2	Little Mermaid	0	11.21	29.2	−0.54	−1.08	NA	0.08	1.90	8.6E−03		
OM12_02K	Falaij 2	Flounder	3.5	11.27		−0.51	−0.93	−12.85	0.15	1.89	BDL		
OM12_02J	Falaij 2	Sebastian	5.9	11.28		−0.36	−0.25	−14.95	0.14	1.81	8.8E−03		
OM12_02I	Falaij 2	Ursula	10.2	11.27		−0.11	0.76	−22.86	0.18	1.52	1.0E−02		
OM12_02H	Falaij 2	Triton	13.7	11.32		−0.11	0.79	−21.30	0.15	1.45	BDL		
OM08_W 14	Masira			11.26		−1.65	−8.35						
OM09_W10U	Misbit	Misbit Spring		11.37	31.4	−1.11	−6.63	−15.11	0.38				OM11_07U,V
OM10_01A	Misbit	Misbit Spring		11.2	31.6	−1.39	−6.75	−5.96	0.24	2.12	1.7E−02	√	OM11_07U,V
		Misbit Spring		11.23	27.4								OM11_07U**,V**
		Misbit mixing		10.62	27.7								OM11_07Y**
OM08_W 18	Qafeefah			11.18		−0.52	0.79						
OM09_W05L	Qafeefah	Eden		11.89	23.8	0.39	−0.92	−20.76	0.38	1.66	6.5E−02	√	
OM10_04S	Qafeefah	Glazed Kidney		11.76	27.5	0.56	4.14	−13.71	0.18	1.75	1.9E−02	√	OM10-1COPS
OM10_04U	Qafeefah	Snail		11.71	24.9	0.28	2.38	−6.19	0.24	1.69	1.9E−02	√	
OM10_07AJ	Shumayt	The Triangle		11.46	33.4	−1.44	−3.49	−17.79	0.12	1.87	2.1E−02	√	
OM10_09AT	Sudari	Chain of Fools		11.61	30.4	−1.54	−6.36	−15.35	0.12	1.78	1.9E−02	√	
OM09_W15J	Uqaybah	Edwin I		11.25	17.6	−1.20	−6.60	−16.14				√	
OM09_W15K	Uqaybah	Edwin II		11.68	21.7	−0.86	−8.49	−13.71					

[a] Rows without water sample ID numbers indicate field measurements.
[b] Site names refer to individual pools at alkaline springs, including source pools and pools along flow paths.
[c] Distance from source spring along flow path over travertine surface.
[d] Limits of detection: DIC – 0.02 mmol/L, Ca – 0.04 mmol/L, Mg – 4.10E−03 mmol/L.
[e] Check mark in "Paukert" column indicates that additional water chemistry data for this sample can be found in Paukert et al. (2012).
[f] Carbonate samples listed in this column were collected at the same site as the corresponding water sample, but not necessarily at the same time. Single or double asterisk indicates that the carbonate was collected at the same time as the water sample.
[*] Carbonates with δ18O and δ13C analyses only (University of Waterloo).
[**] Carbonates with full clumped isotope analyses (WHOI).

measurements and/or Δ_{47} values differed significantly (up to 0.11‰) from other replicate measurements. These discrepancies were due to variations in the He carrier gas flow rate prior to installation of a mass flow controller. As a result, only two replicates are included in the averages for two of the travertine samples because insufficient sample material remained for additional replicate measurements.

Pure CO_2 gases of different bulk isotope compositions equilibrated at 1000 °C and 25 °C or 40 °C (commonly referred to as 'heated gases' and 'equilibrated gases') were analyzed on a daily basis during all three analytical sessions, to correct for instrument nonlinearities and to construct the absolute reference frame (Huntington et al., 2009; Dennis et al., 2011). For heated gases, aliquots of CO_2, including isotopically depleted CO_2 derived from Oman travertine sample OM07-34C, were sealed in quartz tubes and heated in a muffle furnace set at 1000 °C for at least 1 h. Equilibrated gases consisted of CO_2 equilibrated with water maintained at either 40 °C prior to May 2014 (sessions 1 and 2) or 25 °C subsequently (session 3). Two in-house carbonate standards, NBS-19 and 102-GC-AZ01, were also analyzed on a nearly daily basis to monitor system stability within each analytical session and to evaluate potential inter-laboratory differences in clumped isotope measurements.

Carbonate clumped isotope data from these sessions were projected into the absolute reference frame of Dennis et al. (2011), based on the heated and equilibrated gases analyzed during a given session (See Supplementary Table S1 for heated and equilibrated gas analyses, slopes, and intercepts for each session). During the first analytical session, the flow rate of the He carrier gas during the GC purification step occasionally drifted to lower values (e.g., 24 ml/min instead of 30 ml/min). This resulted in significantly higher measured values of $\delta^{13}C$, $\delta^{18}O$, and Δ_{47} for some heated gas and carbonate analyses. These data were excluded from the construction of the gas reference frame for this session, but are still reported in Supplementary Table S1 for reference. Addition of a mass flow controller to maintain the He flow at 30 ± 1 ml/min eliminated this problem in subsequent analytical sessions. By convention, carbonate Δ_{47} values are normalized to acid digestions performed at 25 °C by addition of an acid digestion correction factor. We use an acid digestion correction factor of 0.092‰, determined by Henkes et al. (2013) where the analytical setup was very similar to that used for our analyses at WHOI.

Measurements of two in-house carbonate standards in the three analytical sessions yielded Δ_{47} values of 0.391 ± 0.019‰ (1 S.D., $n = 8$), 0.422 ± 0.021‰ ($n = 17$) and 0.424 ± 0.016‰ ($n = 12$) for NBS19, and 0.725 ± 0.018‰ ($n = 28$), 0.737 ± 0.020‰ ($n = 30$) and 0.733 ± 0.024‰ ($n = 13$) for 102-GC-AZ01, respectively. These values are either within or close to the range of the average values reported in a recent inter-laboratory study, 0.392 ± 0.017‰ (1 S.D.) for NBS19 and 0.713 ± 0.12‰ (1 S.D.) for 102-GC-AZ01 (Dennis et al., 2011). The inter-laboratory difference in clumped isotope measurements is currently a subject of extensive investigation in the clumped isotope community, and is suspected to be related to the difference in the exact analytical protocols in different laboratories (e.g., during the acid digestion process, Came et al. 2014; Defliese et al., 2015).

To account for these inter-laboratory difference in clumped isotope measurements, we applied an additional correction to our clumped isotope data in this study, based on a linear function required to bring these carbonate standards' clumped isotope values in each session into agreement with their previously reported values (Spooner et al., 2016). This approach is similar to the method Dennis et al. (2011) outlined for constructing a secondary reference frame based on carbonate standards. The robustness of this correction procedure has been evaluated in a recent inter-laboratory comparison exercise between the WHOI and Caltech laboratories, where the same powdered carbonate samples were distributed and analyzed at both labs (Spooner et al., 2016). Excellent agreement was observed between the two labs, when the WHOI data were corrected based on the reported Δ_{47} values for NBS19 and 102-GC-AZ01 obtained at Caltech (0.392‰ and 0.724‰ respectively; Dennis et al., 2011; Spooner et al., 2016). We adopt the same reported Δ_{47} values for these two standards during the data correction in this study. Note, the magnitude of this additional correction, an average of 0.005‰ and up to a maximum of 0.015‰, is over one order of magnitude smaller than the range of Δ_{47} variations observed in our carbonate samples (0.21‰; see Section 4.3.2), and thus it should not affect the conclusion of this study.

4. RESULTS

4.1. Alkaline spring conditions

Physiochemical conditions of the alkaline spring water, including temperature, pH, $\delta^{18}O_{water}$, δD, $\delta^{13}C_{DIC}$, and concentrations of DIC, Mg^{2+}, and Ca^{2+}, are reported in Table 2 and plotted in Figs. 3 and 4 and Supplementary Figs. S1 and S2.

Spring water temperatures and pH values measured in this study range from 21.7 to 32 °C and from 11.2 to 12.1, falling within the temperature and pH ranges previously reported for hyperalkaline springs in Oman (i.e., 17–39 °C and 11.0–12.0 for hyperalkaline springs that have not mixed with wadi water; Neal and Stanger, 1985; Paukert et al., 2012; Chavagnac et al., 2013b). The subset of these measurements that were made at the time of collection of fresh carbonate precipitates range from 22.5 to 28.7 °C and from 11.2 to 11.6. Some springs were sampled in the same location in multiple years, demonstrating inter-annual variability up to 4.2 °C and 0.4 pH units (see samples from the same "Site" in Table 2). All the water samples analyzed in this study were collected in January, but seasonal variations in the spring water temperature and pH observed in previous studies were small. For example, year-round observations of one hyperalkaline spring yielded temperatures of 31–36 °C and pH of 11.4–11.8 with the exception of rare influxes of fresh surface waters (Neal and Stanger, 1985). Note that carbonate precipitation may also occur where alkaline spring waters mix with wadi (stream) waters, yielding pH values between 9 and 11 (Paukert et al., 2012; Chavagnac et al., 2013a), but only

Table 3
Stable and clumped isotope data in fresh precipitates and travertine deposits.

Type	Sample	Major carb min	n	$\delta^{13}C$, ‰ VPDB	$\delta^{18}O$, ‰ VPDB	Δ47, ‰
Fresh precipitates from alkaline springs – clumped isotope analyses (WHOI)						
OM10-6COPS	Bottom floc, man-made	Calcite	7	−23.58 ± 0.15	−13.98 ± 0.11	0.826 ± 0.005
OM12_07V	Bottom floc, shallow flow	Calcite + aragonite	3	−24.47 ± 0.12	−16.40 ± 0.11	0.830 ± 0.009
OM12_07X2	Bottom floc, pool	Calcite + aragonite	6	−20.85 ± 0.23	−13.20 ± 0.09	0.883 ± 0.006
OM12_09AA	Bottom floc, shallow flow	Calcite, aragonite	3	−23.90 ± 0.16	−14.13 ± 0.13	0.816 ± 0.011
OM12_09AE	Bottom floc, shallow pool	Calcite + aragonite	6	−16.60 ± 0.11	−12.49 ± 0.09	0.819 ± 0.005
OM11_07U	Bottom floc, pool	Calcite, aragonite	6	−13.23 ± 0.05	−3.50 ± 0.04	0.771 ± 0.007
OM11_07V	Surface film	Calcite, aragonite	6	−27.17 ± 0.05	−16.70 ± 0.05	0.851 ± 0.006
OM11_07Y	Bottom floc, wadi mixing	Aragonite, calcite	3	−13.97 ± 0.02	−4.24 ± 0.09	0.757 ± 0.006
OM09-6COPS	Bottom floc, pool	Aragonite	3	−15.18 ± 0.18	−3.61 ± 0.33	0.750 ± 0.016
OM09-7COPS	Bottom floc, pool	Aragonite	4	−18.53 ± 0.07	−6.99 ± 0.09	0.820 ± 0.011
OM10-1COPS	Surface film	Calcite	6	−26.38 ± 0.03	−16.07 ± 0.30	0.851 ± 0.012
OM10-2COPS	Bottom floc, pool	Aragonite	6	−12.25 ± 0.12	0.22 ± 0.02	0.751 ± 0.007
OM09-8COPS	Bottom floc, pool	Calcite, aragonite	6	−21.42 ± 0.11	−10.33 ± 0.17	0.773 ± 0.008
OM09-10COPS	Surface film	Calcite	3	−23.44 ± 0.35	−14.44 ± 0.03	0.844 ± 0.014
Fresh precipitates from alkaline spring flow paths – $\delta^{13}C$ and $\delta^{18}O$ analyses only (University of Waterloo)						
OM12_07U	Bottom floc		2	−24.54	−16.63	
OM12_07V	Bottom floc		1	−22.99	−16.90	
OM12_07W1	Surface film		2	−24.73	−16.12	
OM12_07W2	Bottom floc		2	−22.60	−15.68	
OM12_07X1	Surface film		2	−25.76	−16.36	
OM12_07X2	Bottom floc		2	−25.13	−12.25	
OM12_01A	Bottom floc		1	−14.90	−6.23	
OM12_01B	Bottom floc		2	−14.59	−4.65	
OM12_01C1	Surface film		1	−21.34	−16.88	
OM12_01C2	Bottom floc		2	−14.35	−5.97	
OM12_01D	Bottom floc		2	−14.06	−4.67	
OM12_01E1	Bottom floc		2	−14.49	0.08	
OM12_01E2	Surface film		1	−24.41	−18.41	
OM12_01F1	Surface film		2	−24.31	−12.99	
OM12_01F2	Bottom floc		2	−10.52	3.14	
OM12_01G1	Surface film		2	−23.58	−14.65	
OM12_01G2	Bottom floc		1	−19.93	−11.76	
Travertine deposits – clumped isotope analyses (WHOI)						
OM08-200	Recent travertine	Calcite	3	−19.98 ± 0.26	−12.06 ± 0.14	0.828 ± 0.007
OM07-34c	Recent travertine	Calcite	6	−25.35 ± 0.06	−15.42 ± 0.04	0.855 ± 0.008
OM09-85C	Recent travertine	Calcite	2	−24.89 ± 0.07	−14.25 ± 0.01	0.839 ± 0.003
OM09-89C	Recent travertine	Calcite	2	−21.85 ± 0.15	−12.05 ± 0.14	0.784 ± 0.019
OM10-32C-1	Travertine terrace	Calcite	3	−17.84 ± 0.05	−7.57 ± 0.05	0.705 ± 0.014
OM10-32C-2	Travertine terrace	Calcite	3	−14.87 ± 0.07	−6.50 ± 0.04	0.675 ± 0.006
OM10-32C-6	Travertine terrace	Calcite	3	−20.75 ± 0.04	−10.60 ± 0.02	0.675 ± 0.006
OM10-32C-8	Travertine terrace	Calcite	3	−16.64 ± 0.15	−9.16 ± 0.13	0.805 ± 0.011
OM10-32C-9	Travertine terrace	Calcite	3	−18.13 ± 0.06	−10.32 ± 0.03	0.787 ± 0.014
OM10-32C-10	Travertine terrace	Calcite	3	−10.87 ± 0.06	−3.86 ± 0.03	0.830 ± 0.010
OM10-32C-11	Travertine terrace	Calcite	3	−3.76 ± 0.07	0.58 ± 0.05	0.790 ± 0.007
OM11-78C-3	Travertine terrace	Calcite	3	−18.80 ± 0.04	−11.67 ± 0.01	0.795 ± 0.003
OM11-78C-4	Travertine terrace	Calcite	3	−19.68 ± 0.43	−12.57 ± 0.30	0.794 ± 0.010
OM11-78C-6	Travertine terrace	Calcite	3	−5.28 ± 0.07	−3.70 ± 0.06	0.695 ± 0.003

All values corrected to carbonate standards for clumped isotope analyses, as described in text.
Reported uncertainties for clumped isotope data are 1-S.E. of replicate measurements.
External precision for bulk stable isotope compositions measured at the University of Waterloo is 0.2‰ (1-S.D.) for $\delta^{18}O$ and 0.1‰ (1-S.D.) for $\delta^{13}C$.

one of the fresh carbonate precipitates we analyzed (OM11_07Y) was formed at such a location (“Misbit mixing”) with a pH of 10.6 (Table 2).

$\delta^{18}O_{water}$ values of hyperalkaline springs measured in this study range from −1.5‰ to 2.5‰ VSMOW, with an average of 0.1 ± 1.0‰ VSMOW (1 S.D.), consistent with previously published oxygen isotope compositions of hyperalkaline springs in Oman (e.g., average of −1.1 ± 0.8‰ VSMOW (1 S.D.); Neal and Stanger, 1985). δD_{water} values of hyperalkaline springs measured in this study range from −8.5‰ to 9.8‰ VSMOW and are strongly correlated with $\delta^{18}O_{water}$. The isotopic composi-

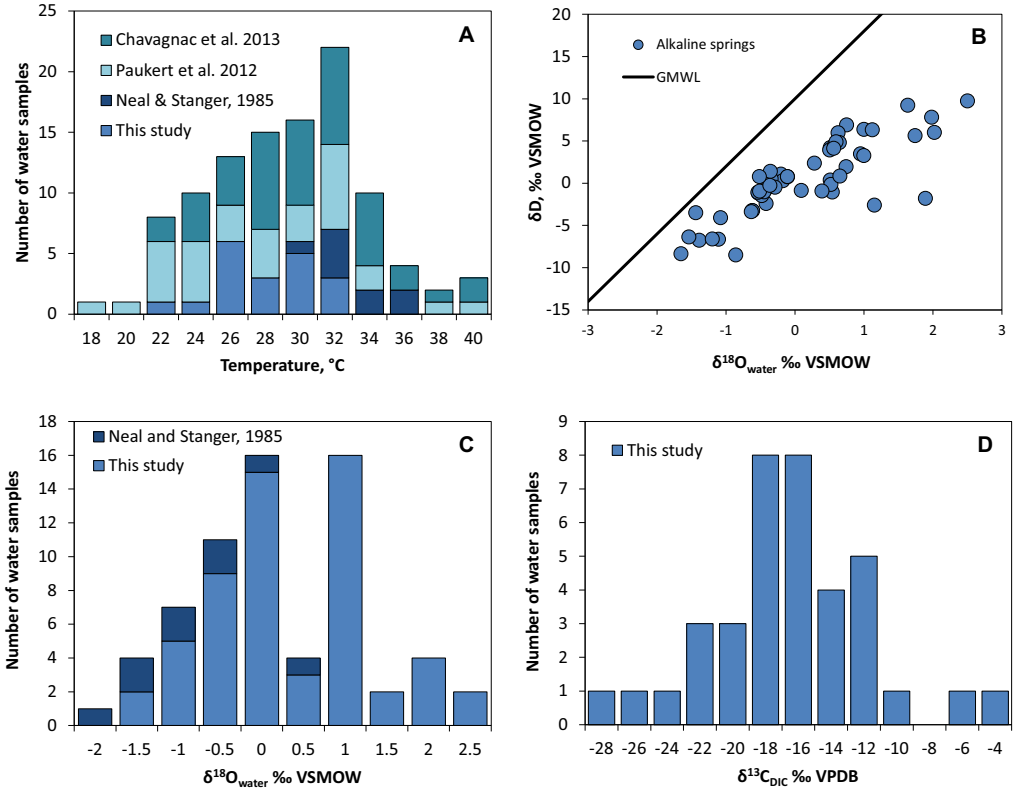

Fig. 3. Water data from hyperalkaline springs in Oman. (A) Distribution of water temperatures at multiple sites measured in January (this study; Paukert et al., 2012; Chavagnac et al., 2013b) and measured year-round at a single site (Neal and Stanger, 1985). (B) Correlation between δD and $\delta^{18}O$ of spring water, shown relative to the global meteoric water line (GMWL) (Craig, 1961). (C) Distribution of $\delta^{18}O$ values of hyperalkaline spring water. (D) Distribution of $\delta^{13}C$ values of dissolved inorganic carbon in hyperalkaline springs.

tions of spring waters lie below the global meteoric water line (GMWL), suggesting evolution along evaporative trends (Fig. 3, Craig, 1961). $\delta^{13}C_{DIC}$ values in hyperalkaline springs range from −28.7‰ to −6.0‰ VPDB, with an average of -17.6 ± 4.8‰ (1 S.D.). Inter-annual variability of the isotopic composition of water at individual springs is smaller than the variability between different springs. $\delta^{18}O_{water}$, δD_{water} and $\delta^{13}C_{DIC}$ values measured in the same pools in different years differ from one another by 0.1‰ to 1.7‰, 1.1‰ to 7.4‰ and 0.04‰ to 9.2‰, respectively (Table 2).

The chemical and isotopic composition of water samples collected along flow paths emanating from a single alkaline source spring and traveling in shallow flows along the surface of travertine terraces exhibit some characteristics indicating combined effects of progressive evaporation, CO_2 uptake, and carbonate precipitation, but there are no systematic trends common to all flow paths (Fig. 4, Fig. S2). For example, $\delta^{18}O_{water}$ and δD_{water} are strongly correlated and increase along evaporative trends for some flow paths. pH also decreases with greater distance from the source spring, as would be expected during CO_2 uptake or carbonate precipitation, for some but not all flow paths (Fig. S2). Similarly, for the two flow paths where DIC concentration data are available, DIC concentration increases slightly overall along the flow paths. Ca concentration generally decreases along the flow path, as would be expected with precipitation of calcium carbonate. Mg concentration remains constant, or increases for flow paths where correlated increases in $\delta^{18}O_{water}$ and δD_{water} suggest progressive evaporation (Fig. S2).

4.2. Carbonate mineralogy and ^{14}C ages

Carbonate minerals identified by XRD and Raman spectroscopy analysis are presented in Table 1. Fresh precipitates in this study are composed of pure calcite, pure aragonite, and mixtures of calcite and aragonite, with calcite more common in crusts formed at pool surfaces and aragonite more common in fine precipitates found lining alkaline pools and spring outlets. This distribution of calcite and aragonite is consistent with the mineralogy observed in other hyperalkaline springs in Oman (Chavagnac et al., 2013a). In contrast, preserved travertines are predominantly calcite, with minor amounts of aragonite found only in one recently-formed travertine sample (OM09-89C).

The calibrated ^{14}C ages of fresh carbonate precipitates and of travertine deposits considered in this study, range from modern to 350 years and from modern to 45,000 years, respectively, where "modern" is defined by >95% of the ^{14}C activity for AD 1950 (Olsson, 1970; Kelemen and Matter, 2008; Kelemen et al., 2011; Mervine et al., 2014; this study). Two of the travertine subsamples (OM10-32C-8 and OM10-32C-10) dated by Mervine et al. (2014) were re-analyzed in this study, yielding calibrated

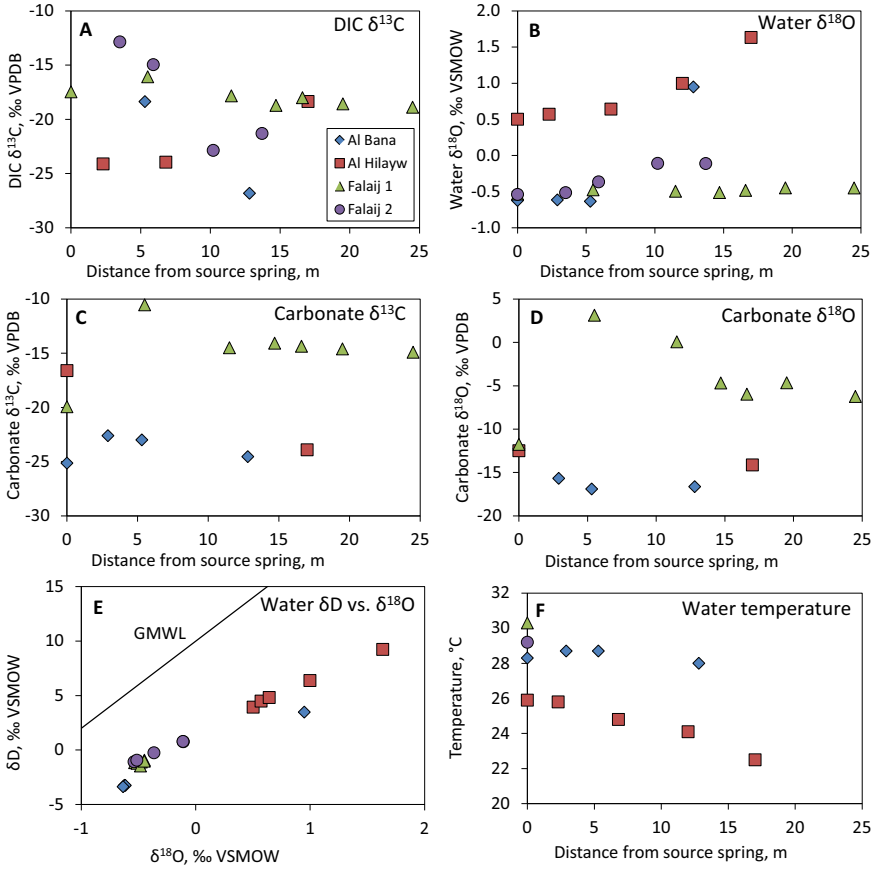

Fig. 4. Stable isotope variations in spring water and carbonate bottom floc along flow paths at Al Bana, Al Hilayw, Falaij 1, and Falaij 2 travertines. There are no systematic variations in $\delta^{13}C$ in spring water DIC (panel A) or carbonate bottom floc (panel C). Spring water $\delta^{18}O$ increases with distance along some flow paths (panel B) and is likely the result of evaporation along the flow path, which also results in enrichments in δD (as shown by the correlation between δD and $\delta^{18}O$ of spring water below the global meteoric water line (GMWL) (Craig, 1961) in panel E). Carbonate $\delta^{18}O$ in bottom floc sampled along flow paths (panel D) does not show systematic variation with distance, $\delta^{18}O_{water}$, or water temperature.

^{14}C ages of 18,350 ± 118 (1 S.D.) years and 15,640 ± 126 years, respectively. These ages are different from their previously reported calibrated ^{14}C ages (16,710 ± 133 years and 23,710 ± 215, respectively; Mervine et al., 2014), which could be related to heterogeneity of the travertine samples. Because the ^{14}C analyses in this study were performed on the same aliquots of sample powders used in the clumped isotope analyses, we refer to these ^{14}C ages in Table 1 and in the following discussion.

4.3. Stable isotope compositions of carbonates

We present the results of stable isotope analyses ($\delta^{13}C$, $\delta^{18}O$ and Δ_{47}) of fresh carbonate precipitates and preserved travertines in Table 3. Raw data of the clumped isotope analyses, including all analyses of samples, carbonate standards, heated gases, and equilibrated gases, are reported in Supplementary Table S1.

4.3.1. Oxygen and carbon isotope compositions

$\delta^{18}O$ and $\delta^{13}C$ values of fresh carbonate precipitates and preserved travertines range from highly depleted values (e.g., $\delta^{18}O_{VPDB}$ and $\delta^{13}C_{VPDB}$ as low as −16.9‰ and −27.2‰ respectively) to values approaching expected equilibrium with spring waters (e.g., $\delta^{18}O_{VPDB} = 0‰$ and $\delta^{13}C_{VPDB} = -4‰$), with a strong positive correlation between the two (overall $\delta^{13}C$ vs. $\delta^{18}O$ slope of 1.1, $R^2 = 0.83$; Fig. 5A). The $\delta^{18}O$ and $\delta^{13}C$ values recorded in these samples overlap with that observed in previous studies of Oman travertine (−17‰ to +6‰ in $\delta^{18}O$, −33‰ to +3‰ in $\delta^{13}C$, and $\delta^{13}C$ vs. $\delta^{18}O$ slope of 1.3, Clark and Fontes, 1990; Clark et al., 1992; Kelemen et al., 2011; Mervine et al., 2014). The bulk oxygen and carbon isotopic compositions of fresh carbonate precipitate samples collected in 2009–2010 and all of the preserved travertine samples in this study were also analyzed in previous studies. $\delta^{13}C$ and $\delta^{18}O$ derived from our clumped isotope analyses typically fall within 0.3‰ of the previously reported values (Supplementary Fig. S3; Kelemen et al., 2011; Mervine et al., 2014). Greater differences were observed between the isotopic compositions derived from clumped isotope analyses at WHOI and those measured at the University of Waterloo: for the two samples analyzed in both laboratories, measurements made at WHOI were

1.48‰ lower in $\delta^{13}C$ and 0.50‰ higher in $\delta^{18}O$ for OM12_07V and 4.28‰ higher in $\delta^{13}C$ and 0.95‰ lower in $\delta^{18}O$ for OM12_07X2. The source of this discrepancy is unknown, but it suggests that caution should be taken in interpreting small variations in the stable isotope compositions of fresh carbonates along alkaline spring flow paths measured at the University of Waterloo. Regardless, these differences remain small relative to the range of isotopic compositions observed in carbonates formed at hyperalkaline springs in Oman.

The most depleted $\delta^{18}O$ and $\delta^{13}C$ values are observed in fresh carbonate films on alkaline spring surfaces and in recently-formed preserved travertines (pale blue diamonds and green squares in Fig. 5A), but several bottom floc samples also record highly depleted bulk isotopic compositions (dark blue diamonds in Fig. 5A). Isotopic depletions are not restricted only to recently-formed samples. Even travertines as old as 40,000 years may preserve significantly depleted isotopic values, e.g., $\delta^{18}O_{VPDB} \sim -13‰$ and $\delta^{13}C_{VPDB} \sim -20‰$.

Samples at the equilibrium end of the observed $\delta^{13}C$-$\delta^{18}O$ trend consist of several old travertines and a few bottom flocs that line hyperalkaline pools. Their isotopic compositions appear to be in equilibrium with the observed range of present-day spring-water temperatures and $\delta^{18}O$ values and with the carbon isotope composition of soil or atmospheric CO_2 (Tables 2 and 4; Neal and Stanger, 1985; Clark et al., 1992; Matter, 2005). Bottom floc samples exhibit slightly lower $\delta^{13}C$ than the older travertines and are thus closer to the expected equilibrium with vegetation-influenced soil CO_2 than atmospheric CO_2 (Clark and Fontes, 1990; Clark et al., 1992). Note however, caution should be taken when interpreting the isotopic composition of older travertines in the context of the present-day conditions in Oman. Although conditions similar to today may have prevailed during many periods in the past, both temperature and $\delta^{18}O$ of meteoric water have varied in Oman over the past 50,000 years (e.g., Burns et al., 2001; Weyhenmeyer et al., 2000). Thus, older travertine samples that appear to be in equilibrium with present-day spring-water conditions could have formed in equilibrium at times when temperature and stable isotope compositions of water were similar to those observed today, or these samples may have formed under isotopic disequilibrium but re-equilibrated isotopically with similar conditions at a later time.

There appears to be a weak correlation between the mineralogy and stable isotope composition in fresh carbonate precipitates, with calcite more abundant in highly fractionated samples and aragonite more abundant in the samples whose isotopic compositions are closer to isotopic equilibrium. The average $\delta^{18}O$ value of fresh carbonate precipitates composed of >90% aragonite ($n = 3$) is only ~2‰ lower than expected equilibrium values for average spring conditions of $T = 28 \pm 4$ °C, $\delta^{18}O_{water} = 0.1 \pm 1.0‰$ SMOW (1 S.D.), while the average $\delta^{18}O$ value of fresh carbonate precipitates composed of >90% calcite ($n = 3$) is ~12‰ lower than expected equilibrium values for these average spring conditions (Kim and O'Neil, 1997; Kim et al., 2007). The average $\delta^{18}O$ value of fresh carbonate precipitates composed of mixtures of both calcite and aragonite (at least ~20% of each, $n = 8$) is ~8–9‰ lower than expected equilibrium values for these average spring

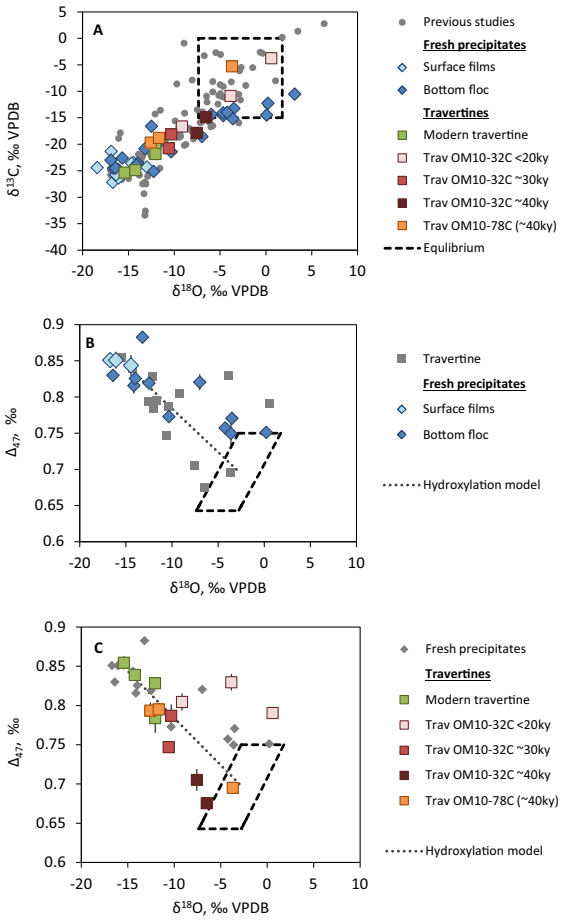

Fig. 5. Clumped isotope and stable isotope results for fresh precipitates (diamonds) and layered travertines (squares). Dashed boxes indicate the range of expected equilibrium values (Table 4). (A) $\delta^{18}O$ and $\delta^{13}C$ values of fresh precipitates and layered travertine in this study overlap with values from previous studies of Oman travertines (gray circles; Clark and Fontes, 1990; Clark et al., 1992; Kelemen et al., 2011; Mervine et al., 2014). $\delta^{18}O$ and $\delta^{13}C$ of fresh precipitates range from highly depleted values in surface films (pale blue diamonds) to more equilibrium-like values in bottom floc (darker blue diamonds), and preserved travertines span a similar range of stable isotope compositions. (B) Clumped isotope compositions of fresh precipitates from alkaline springs range from enriched Δ_{47} values associated with depleted $\delta^{18}O$ values to compositions near expected equilibrium values. Layered travertines (gray squares) are shown for reference. (C) Clumped isotope compositions of layered travertines: recently-formed travertines from active hyperalkaline systems (green squares); subsamples of travertine terrace OM10-32C grouped by ^{14}C age (pink squares <20 ky, medium red squares ~30 ky, dark red squares ~40 ky); subsamples of 40,000 year old travertine terrace OM10-78C (orange squares). Dotted lines in (B) and (C) indicate our first-order theoretical estimation of the Δ_{47}-$\delta^{18}O$ slope associated with CO_2 hydroxylation (). (For interpretation of the references to colour in this figure legend, the reader is referred to the web version of this article.)

conditions, but mixed samples with higher proportions of calcite do not always have larger deviations from equilibrium.

4.3.2. Clumped isotope compositions

Similar to their bulk $\delta^{18}O$ and $\delta^{13}C$ values, Δ_{47} values in fresh carbonate precipitates and preserved travertines also vary significantly, ranging from enriched values (as high as 0.883‰) to values approaching equilibrium with observed alkaline spring temperatures (e.g., observed Δ_{47} as low as 0.750‰ in fresh precipitates and 0.675‰ in preserved travertines compared to expected equilibrium Δ_{47} values of 0.65–0.75‰ for 17–39 °C; Ghosh et al., 2006; Dennis et al., 2011). The magnitude of Δ_{47} enrichments observed in our samples, ~0.13–0.23‰ relative to the expected equilibrium, are similar to those observed in carbonates derived from high-pH laboratory precipitation experiments (~0.12–0.25‰, Schmid, 2011; ~0.26–0.31‰, Tang et al., 2014) and in travertines from hyperalkaline springs in Liguria (~0.19–0.24‰, Schmid, 2011).

We note inter-laboratory difference exists in the calibration of clumped isotope thermometers (e.g., Ghosh et al., 2006; Dennis and Schrag, 2010; Zaarur et al., 2013; Defliese et al., 2015; Kluge et al., 2015). In this study, we discuss our results by reference to the equilibrium clumped isotope values predicted by the calibration of Ghosh et al. (2006) as re-calculated in the absolute reference frame by Dennis et al. (2011). We regard this as the most appropriate calibration for our data at this stage because our data have been normalized to the accepted values of the two in-house carbonate standards at Caltech (Section 3.5.3). High Δ_{47} materials yield higher Δ_{47} values when analyzed at Caltech than in many other labs (Dennis et al., 2011), consistent with the steepness of the Ghosh et al. (2006) calibration produced at Caltech, which appears to remain valid for a wide variety materials analyzed at Caltech regardless of updated digestion procedures at 90 °C (Falk and Kelemen, 2015; Tripati et al., 2015). We therefore consider consistent standard measurements to be a more important factor in choosing an appropriate clumped isotope calibration to apply than acid digestion temperature. More importantly, over the temperature range of spring water in Oman (17–39 °C), the expected equilibrium Δ_{47} values are similar for other existing carbonate clumped isotope calibrations (e.g., Dennis and Schrag, 2010; Zaarur et al., 2013; Defliese et al., 2015; Kluge et al., 2015). The maximum difference in expected equilibrium Δ_{47} values derived from different calibrations is ~0.03‰, much smaller than the range of Δ_{47} variations observed in our samples. Therefore, the choice of clumped isotope equilibrium calibration should not affect the conclusion of this study.

Relative to expected equilibrium values at average ambient temperatures and fluid isotopic compositions ($\delta^{18}O_{water} \sim 0$‰, T ~ 28 °C; Table 2), enrichments in Δ_{47} in fresh carbonate precipitates correlate with depletions in their $\delta^{13}C$ and $\delta^{18}O$, yielding a Δ_{47}-$\delta^{18}O$ slope of −0.011 between samples furthest from isotopic equilibrium and expected equilibrium values (Fig. 5). Crystalline films from alkaline pool surfaces, which show the largest depletions in $\delta^{13}C$ and $\delta^{18}O$, record enriched Δ_{47} values of 0.85 ± 0.01‰ (Fig. 5B), about 0.10–0.20‰ higher than expected for the range of temperatures observed in alkaline springs in Oman (~17–39 °C: Table 2; Paukert et al., 2012; Chavagnac et al., 2013b). These Δ_{47} values correspond to unrealistically low apparent clumped isotope temperatures of ~0 °C (Ghosh et al., 2006; Dennis et al., 2011). Similar disequilibrium isotopic signatures are also observed in some bottom floc samples, with enriched Δ_{47} values of 0.773–0.883‰. In contrast, aragonite-rich bottom floc whose ^{13}C and ^{18}O fall within the range of expected equilibrium values for ambient conditions in Oman record Δ_{47} values of 0.738–0.758‰ (Fig. 5B), corresponding to apparent clumped isotope temperatures of 17–13 °C (Ghosh et al., 2006; Dennis et al., 2011). These apparent temperatures are slightly lower than the lowest spring temperatures measured during the winter field seasons, but are consistent with typical winter air temperatures in Oman (Paukert et al., 2012; Oman Directorate General of Meteorology, 2015).

Clumped isotope compositions of preserved travertines also span a large range of Δ_{47} values, from 0.855‰ to 0.675‰, which correspond to apparent clumped isotope temperatures of −1 °C to 33 °C (Fig. 5C). Similar to their $\delta^{13}C$ and $\delta^{18}O$, Δ_{47} values of recently-formed travertines (i.e., with calibrated ^{14}C ages between modern and 305 years) overlap with those observed in fresh precipitates at the disequilibrium end of the isotopic trends. Some older travertine subsamples (calibrated ^{14}C ages of 18,350–41,610 years) also record disequilibrium $\delta^{13}C$, $\delta^{18}O$, and Δ_{47} values overlapping those observed in recently-formed travertines, while other travertine subsamples (calibrated ^{14}C ages of 34,000–45,000 years) record $\delta^{13}C$, $\delta^{18}O$, and Δ_{47} values between the disequilibrium values observed in recently-formed travertines and values consistent with equilibrium at temperatures of ~35 °C (Kim and O'Neil, 1997; Ghosh et al., 2006; Dennis et al., 2011). Note that some subsampled layers in one travertine outcrop (OM10-32) yield Δ_{47} values higher than expected from the isotopic trends observed in fresh precipitates. These additional enrichments are interpreted to reflect mixing between isotopically distinct generations of carbonate within the travertine layers (see discussion in Section 5.1.3).

5. DISCUSSION

5.1. Fresh calcium carbonate precipitates

5.1.1. Disequilibrium end-member

Among different types of fresh carbonate precipitates, surface films record the greatest extent of stable isotope disequilibrium (e.g., $\delta^{18}O_{VPDB} = -16.7$‰, $\delta^{13}C_{VPDB} = -27.2$‰, $\Delta_{47} = 0.851$‰), but several bottom floc samples from shallow flow paths along travertine surfaces also fall close to this end-member. Note, some of these bottom floc samples may have formed initially as surface films and then settled to the bottom rather than precipitating *in situ*.

Under the high pH conditions observed in alkaline springs, CO_2 uptake and carbonate precipitation is very rapid at the air–water interface. O'Neil and Barnes (1971) proposed that depleted $\delta^{13}C$ and $\delta^{18}O$ values in travertines from alkaline springs in northern California result from

CO_2 diffusion kinetics across the air–water interface. However, Clark et al. (1992) found this mechanism could not fully explain the kinetic isotope effects observed in their high-pH carbonate precipitation experiments and suggested instead that the observed depletions in $\delta^{13}C$ and $\delta^{18}O$ in alkaline spring carbonates are related to the CO_2 hydroxylation reaction. They concluded that depleted $\delta^{13}C$ values in these carbonates were best explained by a kinetic isotope fractionation on the order of 15‰ during hydroxylation, while their depleted $\delta^{18}O$ values resulted from unidirectional reaction of CO_2 with hydroxyl ions, which are isotopically lighter than H_2O molecules by ~40‰ (Green and Taube, 1963). This mechanism was supported by studies of calcite precipitation from high pH solutions (e.g., pH >12, Dietzel et al., 1992; Kosednar-Legenstein et al., 2008), and their estimated carbon isotope fractionation fall within the range from other experimental studies (e.g., 11 to 39‰ over 18–24 °C, Zeebe and Wolf-Gladrow, 2001).

Strong depletions in $\delta^{13}C$ and $\delta^{18}O$ of the surface film samples are accompanied by significant enrichments in their Δ_{47} values. Although the exact mechanism generating these Δ_{47} enrichments cannot be determined from these data alone, it is expected that the CO_2 hydroxylation reaction responsible for depletions in their $\delta^{13}C$ and $\delta^{18}O$ will also produce kinetic enrichments in their clumped isotope compositions (Appendix A). We obtain a first-order estimate on the clumped isotope composition of the HCO_3^- produced from the CO_2 hydroxylation reaction, assuming isotopic composition of the CO_2 is in equilibrium with water and no kinetic isotope fractionation is associated with CO_2 hydroxylation (i.e. random addition of OH^-). Similar assumptions have been employed in previous studies to estimate the oxygen isotope composition of the HCO_3^- derived from this reaction (e.g., Rollion-Bard et al., 2003). Our estimation suggests that, at 300 K, CO_2 hydroxylation leads to enriched clumped isotope compositions of HCO_3^- relative to the expected equilibrium values, with a Δ_{47}-$\delta^{18}O$ slope of −0.012 (See details in Appendix A).

Because CO_2 uptake and carbonate precipitation is rapid at the air–water interface in alkaline springs, there are limited opportunities for oxygen isotope and clumped isotope equilibration of the DIC, especially under those high pH conditions. Therefore, the Δ_{47} values of the carbonates precipitated at the surface of alkaline springs are expected to reflect that of the HCO_3^- derived from the CO_2 hydroxylation reaction and be enriched relative to the expected equilibrium values. The agreement between our theoretically estimated Δ_{47}-$\delta^{18}O$ slope of -0.012 and the Δ_{47}-$\delta^{18}O$ slope of −0.011 observed between surface film samples and values expected in equilibrium with average spring water conditions ($\delta^{18}O_{water} \sim 0$‰, $T \sim 28$ °C; Table 2) further supports CO_2 hydroxylation as the main cause of the observed depletions in $\delta^{18}O$ and $\delta^{13}C$ and enrichments in Δ_{47} (Fig. 5).

5.1.2. Equilibrium end-member

The $\delta^{13}C$, $\delta^{18}O$, and Δ_{47} values of some bottom floc samples are close to the equilibrium values expected for conditions observed in Oman alkaline springs and surface runoff waters. The bottom floc samples with isotopic compositions closest to expected equilibrium values are rich in aragonite. However, calcite and aragonite cannot be strictly assigned as disequilibrium and equilibrium end-members respectively because some surface film samples recording strong disequilibrium isotopic signatures also contain significant proportions of aragonite. Instead, we suggest that aragonite precipitation may be favored relative to calcite under conditions where isotopic equilibrium is also more likely to be achieved.

Chavagnac et al. (2013a) suggest aragonite precipitation may be favored when surface runoff, containing much higher concentrations of Mg^{2+} and DIC than alkaline spring water, reacts with alkaline spring water. This could occur either as surface runoff enters an alkaline pool or when alkaline spring waters seep back into pools that have been flooded with surface runoff. Increases in the Mg/Ca ratio under these conditions could favor precipitation of aragonite rather than calcite, and atmospheric- or soil-derived DIC in the surface runoff could have already equilibrated isotopically before reaction with alkaline fluids, leading to apparent equilibrium values in $\delta^{13}C$, $\delta^{18}O$, and Δ_{47} of the resulting bottom floc. Thus, the isotopic composition of bottom floc samples that appear close to equilibrium could reflect conditions during infrequent surface runoff events (i.e., rainy days) rather than the observed alkaline spring conditions.

It is however important to note that bottom floc samples could represent mixtures of carbonates formed at different times under varying conditions. They may comprise carbonate precipitated at the bottom of the pool, surface films that have broken and settled to the bottom, or carbonate terraces formed on the edge of the pool that have slumped or been washed into the pool. It is also unknown how long these samples have remained at the bottom of the pool before they were collected. Thus, while we can be fairly certain that surface films formed under the observed conditions at the surface of the pools, the conditions at the time of bottom floc precipitation are not necessarily the same as the conditions measured in the alkaline springs at the time of sample collection.

5.1.3. Mixing between disequilibrium and equilibrium end-members

We note that some bottom floc samples with $\delta^{13}C$ and $\delta^{18}O$ compositions intermediate between the most kinetically fractionated values and equilibrium values have Δ_{47} values in excess of linear trends between the enriched disequilibrium values observed in surface films and values representing equilibrium with observed water temperatures (Fig. 6). This suggests that some bottom floc samples, particularly those formed in larger alkaline pools, may represent mixtures between these two isotopically distinct carbonate end-members.

It is known that mixing of two carbonates with different $\delta^{13}C$ and $\delta^{18}O$ may result in a Δ_{47} value of the mixture that is not linear with respect to the proportions of the two end-members (Eiler and Schauble, 2004; Affek and Eiler, 2006; Halevy et al., 2011; Defliese and Lohmann, 2015). The exact Δ_{47} value of the mixture can be higher or lower than the weighted average of the two end-members, depending on the differences in the $\delta^{13}C$ and $\delta^{18}O$ of the

two end-members. For two end-members whose $\delta^{13}C$ and $\delta^{18}O$ values are positively correlated, as in carbonates precipitated at alkaline springs, mixing is expected to lead to a positive Δ_{47} anomaly that is a quadratic function of the mixing ratio and whose magnitude increases with the difference in bulk stable isotope compositions between end-members.

We therefore calculate the expected clumped isotope compositions for mixing between the disequilibrium end-member and several possible equilibrium end-members covering the observed ranges of temperatures in northern Oman, $\delta^{18}O_{water}$ of alkaline spring waters, and $\delta^{13}C$ of soil or atmospheric CO_2 (Fig. 6, Table 4). These calculations show that the bulk stable isotope and clumped isotope compositions of most bottom floc samples from larger alkaline pools (open blue diamonds in Fig. 6) are not consistent with mixing with an end-member that formed under equilibrium with alkaline spring conditions observed at the time of collection. For example, the "Misbit" curve in Fig. 6 does not pass through precipitates collected in that spring (black crosses). Instead, their isotopic compositions are better explained by mixing between the disequilibrium end-member and an equilibrium end-member formed at temperatures of about 17–25 °C and $\delta^{13}C$ of soil CO_2 (Fig. 6). While slightly lower than temperatures typically observed in hyperalkaline spring water in Oman, the temperature of this inferred equilibrium end-member agrees well with average winter air temperatures in northern Oman (e.g., January average daily temperature range of 12–26 °C in Nizwa, Oman Directorate General of Meteorology, 2015), and may reflect the temperature of surface runoff from winter rainfall rather than the temperature of groundwater discharge. Northern Oman currently receives most of its rainfall during the winter months. The agreement of average rainy season temperatures with temperatures of the inferred equilibrium end-members suggests that identifying such equilibrium end-members in old travertines formed in similar environments could help constrain the rainy season temperatures in the past.

Note, one aragonite-bearing sample from the bottom of a large alkaline pool in Wadi Sudari (OM09-8COPS) does not fall on the mixing trend of a low-temperature equilibrium end-member, but instead would require an equilibrium end-member formed at ~40 °C. While it is possible that this sample reflects a carbonate component formed in isotopic equilibrium with rainwater in warmer months, it may be more likely that this sample formed in a shallow flow path along travertine surfaces near the edge of the pool and later washed or slumped into the pool and thus reflect processes other than carbonate mixing (see discussion in Section 5.1.4). The fact that a layered travertine sample collected from the edge of this same pool (OM09-89C) has an isotopic composition extremely close to this sample supports the latter explanation.

5.1.4. Equilibration of DIC

Isotopic variations among many of the fresh precipitates that formed in shallow alkaline spring flows along travertine terraces (filled blue diamonds in Fig. 6) cannot be explained by mixing between the disequilibrium end-member and the low-temperature equilibrium end-member described above. The isotopic composition of these samples lie relatively close to the disequilibrium end-member and do not show obvious curvature in their Δ_{47}-$\delta^{13}C$ and Δ_{47}-$\delta^{18}O$ trends. If we nevertheless seek to explain the variations in isotopic compositions of these samples by invoking carbonate mixing, the equilibrium end-member carbonate would need to have formed above 35 °C. Although such temperatures can be attained in some alkaline springs in Oman, water temperatures measured at the exact collection sites of these specific samples do not exceed 29 °C. Furthermore, these samples were found along the bottom of rivulets and small, shallow pools along the surface of travertine terraces; at these locations there is less opportunity for surface runoff to collect and react with alkaline spring water to form equilibrium end-members than at locations where alkaline springs form larger "blue pools" within stream beds.

Instead, we suggest that the isotope compositions of these samples reflect partial isotopic equilibration of DIC in alkaline pools and surface flows, creating apparent linear Δ_{47}-$\delta^{13}C$ and Δ_{47}-$\delta^{18}O$ trends toward the expected equilibrium values with ambient spring conditions. The carbon isotope compositions of the DIC measured in the Oman alkaline springs support this interpretation. $\delta^{13}C_{DIC}$ in most alkaline springs falls between −13 and −20‰, rather than recording the most extreme kinetic depletions (i.e., $\delta^{13}C$ as low as −27.2‰ VPDB in surface films). The lack of positive correlations between $\delta^{13}C_{DIC}$ and the concentration of DIC or Mg^{2+} (Supplementary Fig. S2) suggests these variations in $\delta^{13}C_{DIC}$ are more likely related to gradual equilibration of initially ^{13}C-depleted DIC in the alkaline pools, as opposed to mixing with surface run-off waters which would have higher concentrations of DIC and Mg^{2+} and more equilibrated isotopic compositions of DIC. However, we do not observe systematic shifts towards equilibrium values in the isotopic compositions of DIC and carbonate precipitates along individual flow paths (Fig. 4). This indicates that the isotope equilibration process does not merely occur incrementally along surface flow paths, but may depend also on other factors which would affect the overall residence time of DIC, such as the rates of CO_2 uptake and carbonate precipitation, water depth, and flow regime.

5.2. Preserved travertines

Laminated travertines with ages ranging from modern to over 40,000 years record many of the same processes recorded by fresh carbonate precipitates at alkaline springs. These include (1) kinetic enrichments in Δ_{47} accompanying depletions in $\delta^{13}C$ and $\delta^{18}O$, associated with hydroxylation of CO_2; and (2) $\delta^{13}C$, $\delta^{18}O$, and Δ_{47} values that trend from this kinetic disequilibrium end-member toward equilibrium values, likely reflecting gradual, partial isotopic equilibration of DIC in the alkaline pools and surface flow paths. However, these highly porous travertines may also be subject to continued interaction with surface waters and alkaline spring waters after their original deposition, which could result in additional modification of their isotopic

Table 4
Possible carbonate mixing end-members for bottom floc.

	T, °C[a]	Δ_{47}, ‰[b]	Water $\delta^{18}O$, ‰ VSMOW[c]	Carbonate $\delta^{18}O$, ‰ VPDB[d]	Carbonate $\delta^{13}C$,‰ VPDB[e]	End-member Abbrev.
Disequilibrium end-member	N/A	0.851	N/A	−16.7	−27	DIS
Equilibrium end-members						
Carbon from soil CO_2	17	0.750	−2.1	−2.8	−15	EM1-1
	17	0.750	2.5	1.8	−15	EM1-2
	39	0.643	−2.1	−7.4	−15	EM1-3
	39	0.643	2.5	−2.8	−15	EM1-4
Carbon from atmospheric CO_2	17	0.750	−2.1	−2.8	0	EM2-1
	17	0.750	2.5	1.8	0	EM2-2
	39	0.643	−2.1	−7.4	0	EM2-3
	39	0.643	2.5	−2.8	0	EM2-4
Misbit Spring	32	0.681	−1.4	−5.0	−6	MS

[a] Minimum and maximum temperatures observed in alkaline springs in Oman (17 and 39 °C, respectively; Table 2; Paukert et al., 2012; Chavagnac et al., 2013b) are used to define extreme equilibrium end-members. Measured temperature in Misbit Spring in 2010 (water sample OM10_01A).

[b] Expected Δ_{47} values (Ghosh et al., 2006) for given equilibrium end-member temperature; measured Δ_{47} value in OM11_07V used as representative disequlibrium end-member.

[c] Minimum and maximum $\delta^{18}O$ values observed in alkaline spring water in Oman (−2.1 and 2.5‰ VSMOW, respectively; Table 2; Neal and Stanger, 1985) used to define extreme equilibrium end-members. Measured spring water $\delta^{18}O$ in Misbit Spring (OM10_01A).

[d] Expected carbonate $\delta^{18}O$ in equilibrium with given $\delta^{18}O_{water}$ value and temperature (Kim and O'Neil, 1997). Measured value in OM11_07V used for disequilibrium end-member.

[e] Extreme end-members defined by minimum and maximum expected carbonate $\delta^{13}C$ in equilibrium with carbon from soil CO_2 and atmospheric CO_2, respectively. Expected carbonate $\delta^{13}C$ in equilibrium with soil CO_2 ranges from approximately −15 to −6‰ VPDB, while expected carbonate $\delta^{13}C$ in equilibrium with soil CO_2 ranges from approximately −3 to 0‰ VPDB (Clark et al., 1992). Measured $\delta^{13}C_{DIC}$ in Misbit Spring (water sample OM10_01A). Measured value in OM11_07V used for disequilibrium end-member.

compositions via recrystallization (dissolution and re-precipitation) and/or precipitation of secondary carbonates within the pore space of the travertine.

5.2.1. Inheritance and preservation of kinetic trends

The recently-formed laminated travertine samples analyzed in this study (^{14}C age ⩽305 years, $n = 4$) preserve significant disequilibrium signatures in their $\delta^{13}C$, $\delta^{18}O$, and Δ_{47} values (Fig. 5). In these travertine samples, the variations of $\delta^{13}C$, $\delta^{18}O$, and Δ_{47} away from the disequilibrium end-member are similar in slope and extent to the trends attributed to partial equilibration of DIC for fresh precipitates, i.e., trends characteristic of fresh precipitates formed in shallow pools and flow paths along travertine terraces. Unlike fresh precipitates formed at the bottom of larger "blue pools," none of the recently-formed travertine samples record isotopic compositions close to possible equilibrium values. These four samples may not be representative of all recently-formed travertines and may reflect a sampling bias. Delicately layered recent travertine samples were collected from exposed surfaces of travertine terraces, similar to the environment of fresh precipitates formed in shallow rivulets and small pools along travertine terraces, rather than larger pools within wadi (stream) beds. They are thus more closely tied to the process of carbonate precipitation in shallow surface flows and crusts formed at the air–water interface than to bottom floc in pools which are more influenced by occasional surface runoff. Accordingly, we would expect their isotopic composition to reflect the trends associated with kinetic disequilibrium and partial DIC equilibration rather than the non-linear trends associated with mixing with isotopically equilibrated carbonate end-members.

Several of the older travertine subsamples (20,000–40,000 years old) also record $\delta^{13}C$, $\delta^{18}O$, and Δ_{47} values that overlap with the kinetic trends observed in fresh precipitates, demonstrating that disequilibrium clumped isotope signals can be preserved over these time scales and that the same processes operating in the active system today are responsible for the formation of extensive fossil travertine terraces. However, the $\delta^{13}C$, $\delta^{18}O$, and Δ_{47} of some older travertine subsamples extend beyond the range observed in fresh precipitates and recently-formed travertines along the DIC equilibration trend and closely approach the range of values expected for equilibrium with present-day ambient conditions in alkaline springs. Note, $\delta^{18}O$ values of meteoric water in Northern Oman may have been up to 6‰ lower than present-day values during previous interglacial periods (Burns et al., 2001), and groundwater temperatures may have been about 6 °C cooler during the late Pleistocene (Weyhenmeyer et al., 2000). However, even taking into account these variations, the isotopic compositions of these carbonate samples would still appear to be close to equilibrium with paleo-conditions. We suggest isotopic exchange during post-depositional recrystallization may be responsible for shifting the isotopic composition of these travertine samples towards equilibrium values, as they interact with surface- and ground-waters. Most fresh precipitates at alkaline springs contain at least minor amounts of aragonite, but aragonite is absent from all older

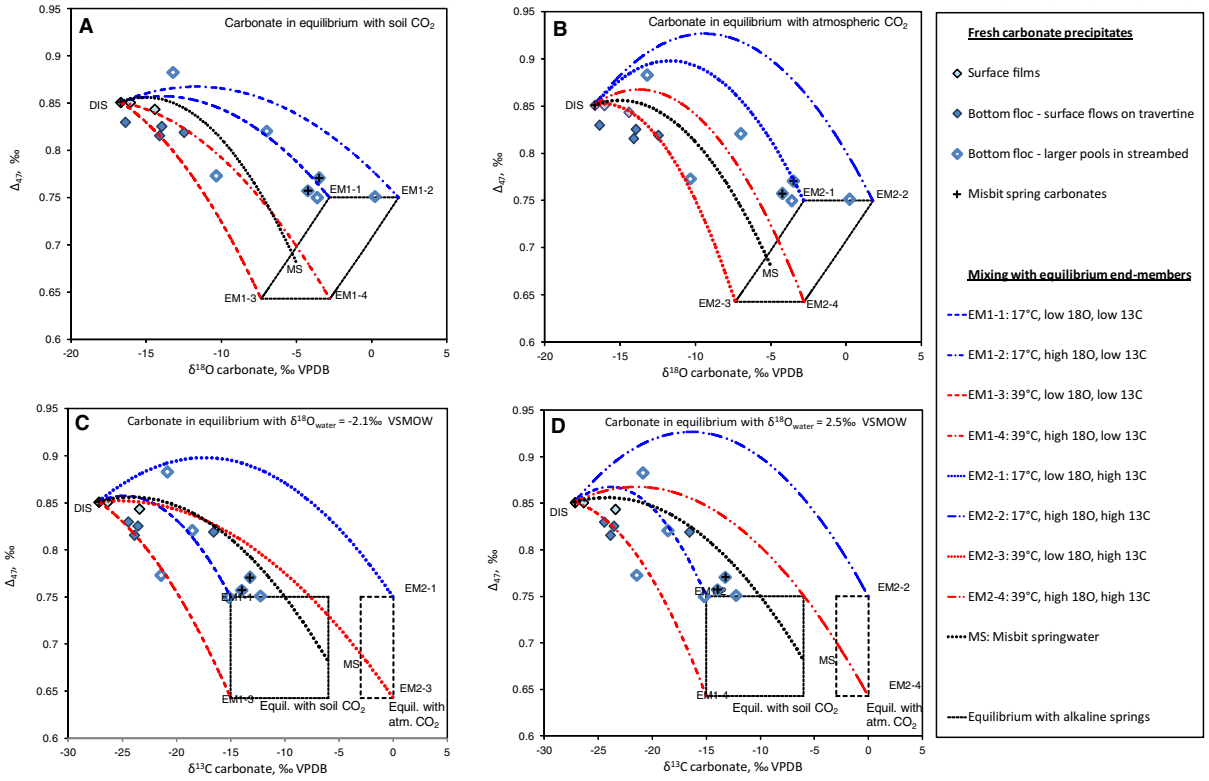

Fig. 6. Mixing trends in fresh precipitates from alkaline springs. Each panel shows Δ47-$\delta^{18}O$ mixing trends between the disequilibrium end-member (i.e., surface films) and several possible equilibrium end-members: (A) equilibrium with the lowest $\delta^{13}C$ values expected in soil CO_2 (carbonate $\delta^{13}C$ of −15‰ VPDB; Clark et al., 1992), (B) equilibrium with the atmospheric CO_2 (carbonate $\delta^{13}C$ of 0‰ VPDB; Clark et al., 1992), (C) equilibrium with the lowest $\delta^{18}O$ values observed in alkaline springs in Oman (water $\delta^{18}O$ −2.1‰ VSMOW; Neal and Stanger, 1985), (D) equilibrium with the highest $\delta^{18}O$ values observed in alkaline springs in Oman (water $\delta^{18}O$ 2.5‰ VSMOW; this study). Dashed black boxes indicate the range of expected values at equilibrium (Table 4). The black dotted line shown in all panels represents mixing with an equilibrium end-member corresponding to the temperatures and isotopic compositions of alkaline spring water from Misbit Spring, and does not pass through the data points representing fresh carbonate precipitates from that specific spring (black crosses). Most bottom floc samples from larger pools record Δ_{47} values in excess of linear trends between the enriched disequilibrium values observed in surface films and values representing equilibrium with observed water temperatures. These trends are best explained by mixing between a disequilibrium end-member and an end-member formed in equilibrium with somewhat cooler temperatures (e.g., 17–25 °C, corresponding to Δ_{47} values of 0.75–0.71‰) than those typically observed in hyperalkaline springs. (For interpretation of the references to colour in this figure legend, the reader is referred to the web version of this article.)

travertine samples. This is consistent with our suggestion that recrystallization occurred in these older travertine samples and has affected their isotopic compositions.

5.2.2. Mixing with subsequent carbonate precipitates

Based on their ^{14}C ages and isotopic compositions, subsampled layers (within a 1 m section) of travertine terrace OM10-32C can be classified into three groups: (1) subsamples with calibrated ^{14}C ages of ~30 ky, whose $\delta^{13}C$-$\delta^{18}O$-Δ_{47} values fall on the DIC equilibration trend ($n = 2$, medium red squares in Fig. 5); (2) subsamples with calibrated ^{14}C ages of ~40 ky, whose $\delta^{13}C$-$\delta^{18}O$-Δ_{47} values approach equilibrium with present-day ambient conditions ($n = 2$, dark red squares in Fig. 5); and (3) subsamples with calibrated ^{14}C ages of ~9–18 ky, whose $\delta^{13}C$-$\delta^{18}O$-Δ_{47} values deviate significantly from the trends observed in fresh precipitates and recently-formed travertines ($n = 3$, pink squares in Fig. 5). Although the linear correlation in $\delta^{13}C$ and $\delta^{18}O$ of these three younger subsamples overlaps with trends in other travertine samples from this and previous studies (Clark and Fontes, 1990; Clark et al., 1992; Kelemen et al., 2011; Mervine et al., 2014), their enriched Δ_{47} values at intermediate $\delta^{13}C$ and $\delta^{18}O$ values are strongly suggestive of mixing of two carbonate end-members. Specifically, these intermediate clumped isotope compositions are consistent with mixing between travertine along the DIC equilibration trend and another carbonate end-member with higher $\delta^{13}C$ and $\delta^{18}O$, e.g. later generations of carbonate precipitation within the pore space of the travertine (Fig. 7). ^{14}C data from these subsamples also support this interpretation, with modern carbon fractions (F_m) positively correlating with their $\delta^{13}C$ and $\delta^{18}O$ (Fig. 7B). Note, mixing of travertines with a younger carbonate end-member with higher $\delta^{18}O$ could generate correlations between F_m and $\delta^{18}O$, but would not necessarily form a perfect linear correlation line because the travertine subsamples are unlikely to all have formed at the same time.

Mixing between a hypothetical end-member ($\delta^{13}C_{VPDB} = 0‰$, $\delta^{18}O_{VPDB} = 3.9‰$, $\Delta_{47} = 0.738‰$) and

travertine lying along the DIC partial equilibration trend near the isotopic composition of OM10-32C-9 ($\delta^{13}C_{VPDB} = -18.1‰$, $\delta^{18}O_{VPDB} = -10.3‰$, $\Delta_{47} = 0.787‰$) accurately reproduces $\delta^{13}C$, $\delta^{18}O$, Δ_{47} values of all three younger subsamples of OM10-32C when the assumed proportion of the hypothetical end-member in OM10-32C-8, OM10-32C-10, and OM10-32C is 8%, 43%, and 78%, respectively. This hypothetical end-member was derived by extrapolating the observed $\delta^{18}O$-$\delta^{13}C$ correlation in these subsamples (Fig. 7A) to $\delta^{13}C_{carbonate} = 0‰$ VPDB (i.e., the maximum expected equilibrium value based on ambient conditions and carbon sources; Clark et al., 1992), then varying the Δ_{47} of this end-member to obtain the best fit between the calculated mixing curve and the measured Δ_{47} values of the travertine subsamples (Fig. 7D). This hypothetical end-member is consistent with the isotopic composition of a carbonate formed in isotopic equilibrium with atmospheric CO_2 ($\delta^{13}C_{CO2} \sim -7‰$ VPDB; Clark et al., 1992) and $\delta^{18}O_{water} = 5.1‰$ VSMOW at 20 °C. This could represent a realistic scenario where later generations of carbonates precipitate within the pore space of a travertine as pore-water derived from surface waters and/or alkaline spring waters evaporates.

Our results suggest that clumped isotope measurement can be a valuable tool for identifying these kinds of mixing processes, which cannot be readily identified from bulk stable isotope measurements alone. Furthermore, our results suggest measured ^{14}C ages of travertine may reflect not only ages of the initial travertine formation, but also later carbonate precipitation within the pore space. Depending on the age of the later carbonate precipitation, the "true" ages of the above travertine subsamples can be tens of thousands of years older than their measured apparent ^{14}C ages and the relative chronology of these subsamples can also change substantially (see details in Appendix B).

5.3. Summary of processes affecting isotopic compositions of carbonates associated with alkaline springs

In summary, the observed $\delta^{13}C$, $\delta^{18}O$, and Δ_{47} values in fresh carbonate precipitates at alkaline springs and in preserved travertine terraces can be explained by a combination of four main processes (Fig. 8).

(1) Hydroxylation of CO_2. Uptake of atmospheric CO_2 by "Type II" alkaline spring-waters (high pH, extremely low DIC, high [Ca^{+}], low [Mg^{2+}]), via rapid CO_2 hydroxylation reaction, results in strong depletions in $\delta^{13}C$ and $\delta^{18}O$ and enrichments in Δ_{47} of carbonates. Relative to expected equilibrium values for average alkaline spring conditions, the typical depletion in $\delta^{13}C$ and enrichment in Δ_{47} are approximately 1.1‰ and 0.011‰, respectively, for every 1‰ depletion in $\delta^{18}O$. This observed Δ_{47}-$\delta^{18}O$ slope agrees quantitatively with our first-order theoretical estimation about the Δ_{47}-$\delta^{18}O$ correlation associated with CO_2 hydroxylation reaction.

(2) Partial equilibration of DIC. Although most of the atmospheric CO_2 taken up by alkaline spring water is removed rapidly by the precipitation of calcium carbonate, some amount of DIC may remain in the spring water. This residual DIC may gradually equilibrate isotopically at ambient conditions, producing $\delta^{13}C$-$\delta^{18}O$-Δ_{47} trends towards the expected equilibrium values and resulting in intermediate isotopic compositions observed in both fresh precipitates in shallow alkaline spring outlets and layered travertines.

(3) Mixing of different carbonate end-members. (a) When surface runoff enters alkaline pools, DIC in these runoff waters, which should already be isotopically equilibrated with ambient surface conditions, allows for the precipitation of calcium carbonate (mostly aragonite) with equilibrium values of $\delta^{13}C$, $\delta^{18}O$, and Δ_{47}. Bottom floc samples that are a mixture of this runoff-derived carbonate and carbonate formed by direct reaction of atmospheric CO_2 with alkaline spring water, define mixing trends that are characterized by positive mixing anomalies in Δ_{47} and slightly shallower $\delta^{13}C$-$\delta^{18}O$ correlations. The shallower slope of these $\delta^{13}C$-$\delta^{18}O$ correlations reflects greater influence of soil CO_2 in surface runoff waters, whose $\delta^{13}C$ is lower than that of atmospheric CO_2. (b) Non-linear clumped isotope mixing trends are also evident in subsamples of some older travertine specimen, characterizing the mixing between preserved travertines and later generations of carbonate precipitated within their pore spaces. Although such samples may still lie along the typical travertine $\delta^{13}C$-$\delta^{18}O$ correlations, anomalous enrichments of Δ_{47} at intermediate $\delta^{13}C$ and $\delta^{18}O$ values are indicative of mixing between isotopically distinct end end-members.

(4) Recrystallization of preserved travertines. Unlike fresh carbonate precipitates, some preserved travertines record $\delta^{13}C$, $\delta^{18}O$, and Δ_{47} values close to equilibrium with average conditions in alkaline springs and groundwater in Oman. We suggest that these isotope compositions could have been attained by isotopic exchange during post-depositional recrystallization. Other preserved travertines overlap in isotope composition with recently-formed travertines and fresh carbonate precipitates, suggesting that recrystallization affects some, but not all, older travertine terraces. The extent of this recrystallization process may be controlled by the initial carbonate mineralogy (e.g., replacement of aragonite with calcite) and/or changes in hydrology of the travertine terrace over time (e.g., some portions of travertine terraces will be subject to more post-depositional interaction with water than others).

5.4. Potential applications

The overall trends in $\delta^{13}C$, $\delta^{18}O$, and Δ_{47} discussed above can be applied to distinguish alkaline spring processes from other processes generating correlations in carbonate $\delta^{13}C$ and $\delta^{18}O$ and to identify mixing of different carbonate end-members. Both of these are often not possi-

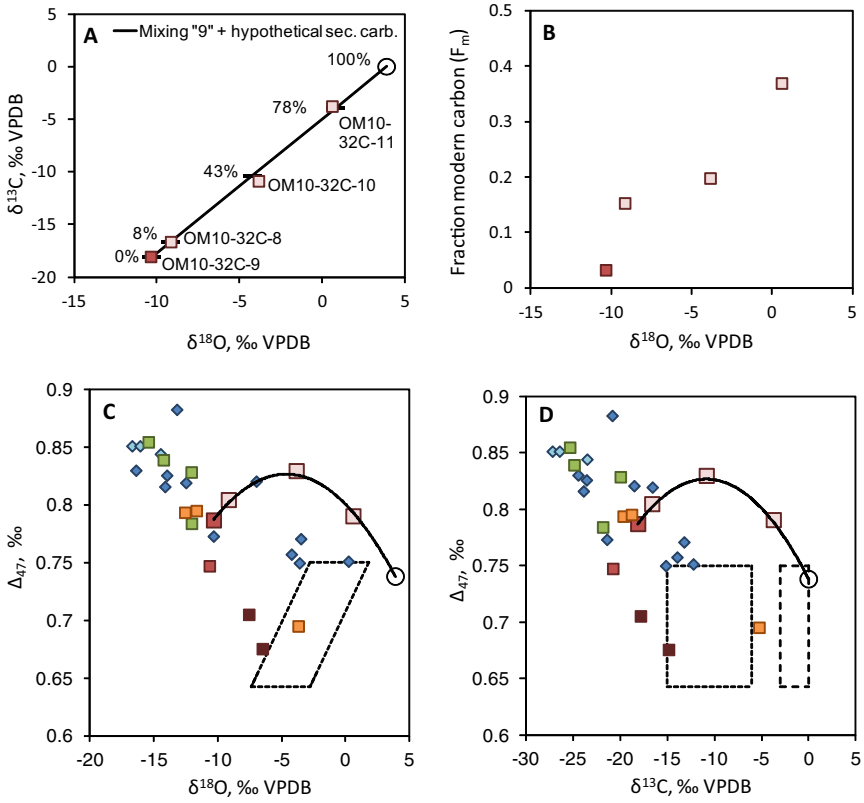

Fig. 7. Mixing trends in young subsamples of OM10-32C. Trends in $\delta^{18}O$, $\delta^{13}C$, fraction modern carbon, and Δ_{47} suggest subsamples of the layered travertine terrace OM10-32C with ages <20 ky represent mixing of two isotopically distinct carbonate end-members. Sample symbols and dashed boxes denoting equilibrium conditions as in Fig. 5. A mixing line (solid black line) between primary travertines with stable isotopic compositions similar to that of OM10-32C-9 and a hypothetical carbonate end-member with higher $\delta^{18}O$ and $\delta^{13}C$ and lower Δ_{47} (open black circle) reproduces the $\delta^{18}O$, $\delta^{13}C$, and Δ_{47} values observed in OM10-32C-8, OM10-32C-10, and OM10-32C with the assumed proportion of the hypothetical endmember in each of these subsample being 8%, 43%, and 78%, respectively (panels A, C, D). Increases in fraction modern carbon would accompany increases in $\delta^{18}O$ and $\delta^{13}C$ due to mixing, but would not produce perfect correlations, as measured ^{14}C ages (panel B) are influenced both by mixing with the younger end-member and real differences in primary travertine ages.

ble when examining the bulk $\delta^{13}C$, $\delta^{18}O$ compositions of carbonates alone.

5.4.1. Identification of carbonate from subaerial hyperalkaline systems

Correlation between enrichments in Δ_{47} and depletions in $\delta^{13}C$ and $\delta^{18}O$ could serve as a marker to identify carbonates formed by rapid uptake of CO_2 in subaerial alkaline environments. $\delta^{13}C$ and $\delta^{18}O$ data alone are insufficient for identifying these processes, as $\delta^{13}C$-$\delta^{18}O$ trends similar in slope and range to those observed in alkaline spring systems can be produced by other processes as well. For example, correlated $\delta^{13}C$ and $\delta^{18}O$ variations are also observed in carbonate cements in conglomerates from Sur, Oman, but are thought to reflect variations in the isotopic composition of surface waters due to past changes in rainfall patterns and vegetation (Burns and Matter, 1995). Because the $\delta^{13}C$-$\delta^{18}O$ trends in those carbonates are not related to the kinetic processes described here, they would be expected to record equilibrium Δ_{47} values. Similarly, it might be unclear in some cases whether depletions in carbonate $\delta^{13}C$ and $\delta^{18}O$ are due to kinetic effects associated with uptake of CO_2 in alkaline environments or inherited from dissolution of carbonate bedrock, e.g., calcium carbonates precipitated during weathering of ultramafic mine tailings (Wilson et al., 2009). Clumped isotope analysis could be a useful diagnostic in these cases. If depletions in $\delta^{13}C$ and $\delta^{18}O$ correlate with enrichments in Δ_{47}, kinetic effects during hydroxylation of CO_2 would be indicated.

This same correlation between $\delta^{18}O$ and Δ_{47} could also be applied to identify extinct alkaline spring systems in terrestrial and extraterrestrial environments. For example, the slope and magnitude of $\delta^{13}C$-$\delta^{18}O$ variations in carbonates in Martian meteorites are similar to that observed in carbonates from terrestrial alkaline springs, and serpentinization-related hyperalkaline systems have been suggested as possible sources of methane generation and carbonate precipitation on Mars (e.g., Niles et al., 2005; Oze and Sharma, 2005; Ehlmann et al., 2010; Etiope et al., 2013; Niles et al., 2013). Identification of a Δ_{47} trend in Martian carbonates similar to trends observed in fresh precipitates and associated travertines in Oman could suggest that hyperalkaline springs were present on the surface of Mars, and may provide further constraints on surface environments on Mars. In one clumped isotope study of Martian carbonates, no such correlation was observed (Halevy et al., 2011). However, as a result of the precious nature of these Martian samples and the challenges to

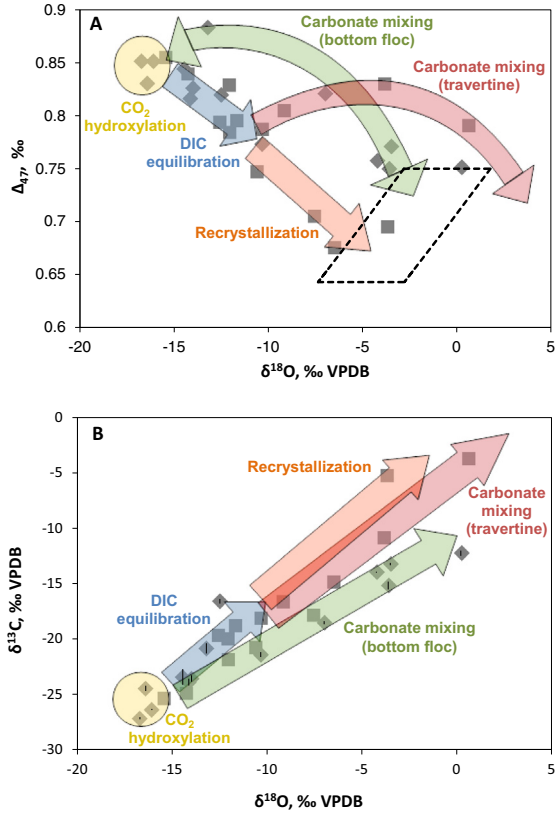

Fig. 8. Processes controlling the stable isotope compositions of carbonates formed at hyperalkaline springs (surface precipitates and bottom floc – gray diamonds, travertines – gray squares) can be distinguished by the Δ_{47} and $\delta^{18}O$ trends they produce (panel A), but largely overlap in $\delta^{18}O$ and $\delta^{13}C$ trends (panel B). These processes include: (1) CO_2 hydroxylation produces enrichments in Δ_{47} and depletions $\delta^{18}O$ and $\delta^{13}C$ (yellow). (2) Partial equilibration of DIC in alkaline springs shifts isotopic composition of the resulting carbonates from the disequilibrium end-member towards equilibrium with ambient conditions (blue). (3) Mixing of isotopically distinct carbonate end-members results in mixing anomalies in clumped isotope composition. For example, alkaline pool bottom floc can include mixtures of the high pH disequilibrium end-member and carbonate precipitated in equilibrium with surface runoff (green). Similarly, the mixing between the travertines and subsequent generations of carbonate that precipitate within the pore space of travertines (e.g., from pore waters with $\delta^{18}O$ enriched by evaporation) can also result in mixing anomalies in clumped isotope composition (red). (4) Carbonate recrystallization (dissolution and re-precipitation) and isotopic exchange in older travertines (orange). (For interpretation of the references to colour in this figure legend, the reader is referred to the web version of this article.)

perform the clumped analysis on such small amounts of samples, only a relatively small range of $\delta^{13}C$ and $\delta^{18}O$ variations were observed in the limited number of analyses in that study (7.8‰ and 5.9‰ respectively), which could obscure variations in Δ_{47} expected from the kinetic trends.

5.4.2. Mixing trends: Identification of carbonate mixing and paleoclimate reconstruction

Due to the non-linear nature of mixing in Δ_{47}, clumped isotope anomalies can be one of the clearest indicators of mixing between carbonates with distinct bulk stable isotopic compositions.

In fresh bottom floc samples from larger alkaline pools, we are able to identify a mixing end-member corresponding to equilibrium with temperatures consistent with winter rainfall in Oman. The laminated travertines analyzed in this study are not likely to have formed under similar conditions as these bottom floc samples, and thus do not reflect the same kind of mixing process. However, it is possible that other travertines in Oman have formed in a pool-bottom environment and would preserve the mixing signatures with an equilibrium end-member recording rainy season conditions. In its current arid climate, Oman receives most of its rainfall in the winter months, but it has experienced wetter climates in the past where rainfall was dominated by the summer monsoon (Clark and Fontes, 1990; Burns et al., 2001; Fleitmann et al., 2003). Carbonate formed in pool bottoms of alkaline springs during those periods could record a mixing end-member in equilibrium with summertime temperatures, allowing identification of major shifts in precipitation patterns that are not available from their bulk stable isotope compositions.

Δ_{47} mixing trends observed in the subsamples of our older travertine samples, reflecting influence of later generations of carbonate precipitation, suggest caution needs to be taken when interpreting ^{14}C age and paleoclimate data from travertines formed at alkaline spring outlets (Appendix B). The non-linear nature of Δ_{47} mixing makes it a valuable tool to identify suites of samples that have been affected by later generations of carbonate precipitation, which is not readily apparent from the $\delta^{13}C$-$\delta^{18}O$ trends alone. Conversely, travertines whose Δ_{47} reflect the same processes observed in fresh precipitates at alkaline springs are likely to provide robust ^{14}C ages and information about their formation conditions.

6. CONCLUSIONS

Carbonates precipitated during atmospheric CO_2 uptake by hyperalkaline springs in Oman record significant enrichments in Δ_{47} correlated with depletions in $\delta^{13}C$ and $\delta^{18}O$. These kinetic isotope effects are the result of hydroxylation of CO_2 under high pH conditions and are best reflected in fresh calcite films formed at the air–water interface. Partial equilibration of the DIC in alkaline springs may shift the clumped isotope and bulk stable isotopic compositions of some bottom floc samples away from this most fractionated end-member along a trend toward expected equilibrium values. These processes are reflected in both fresh precipitates from alkaline springs and associated preserved travertines, though some older travertines may have experienced isotopic re-equilibration.

Because mixing is nonlinear in Δ_{47}, mixing of two isotopically distinct carbonates can be distinguished from equilibration trends or other processes that can also cause correlated variations in $\delta^{13}C$ and $\delta^{18}O$. In fresh bottom floc samples from hyperalkaline springs in Oman, this allows us to identify mixing between the above disequilibrium end-member and possible equilibrium end-members. The nonlinear nature of the clumped isotope signature during mixing

also makes it possible to identify travertine samples that may have been affected by later generations of carbonate precipitation within the travertine pore spaces. The presence of such subsequent carbonate precipitates complicates the interpretation of the ^{14}C age and paleoclimate data from travertines. Mixed samples may not be easily identified from $\delta^{18}O$, $\delta^{13}C$, and ^{14}C trends, whereas Δ_{47}-$\delta^{18}O$-$\delta^{13}C$ trends may show distinctive positive Δ_{47} anomalies at intermediate $\delta^{18}O$ and $\delta^{13}C$ values for samples affected by mixing.

Clumped isotope analysis thus provides a range of details about complex processes occurring during the precipitation and preservation of carbonates at hyperalkaline springs which are not readily apparent from $\delta^{18}O$, $\delta^{13}C$, and ^{14}C data alone.

ACKNOWLEDGMENTS

Special thanks to everyone at the Ministry of Regional Municipalities and Water Resources, Sultanate of Oman, particularly Dr. Abdulaziz Ali-Al-Mashikhi and Salim Al Khanbashi, everyone at the Geological Survey of Oman and the Directorate General of Minerals in the Ministry of Commerce and Industry, particularly Dr. Ali Al Rajhi and Mohammed Al Batashi. Everett Shock, Peter Canovas, Jeff Havig, Jackie Gauntlett, and other members of the Oman field teams are thanked for their assistance with fieldwork and scientific discussions. We thank Dr. Frieder Klein for providing the access to the Raman spectrometer and Dr. Susan Humphris for help in the sample selection. This work was supported by the Howland Postdoctoral Scholarship at WHOI to E. Falk; NSF-ANT-1246387 and the Investment in Science Fund at WHOI to W. Guo; NSF Graduate Research Fellowships to A. Paukert and E. Falk; funding from Petroleum Development Oman, Lamont-Doherty Earth Observatory, and a Columbia Research Initiative in Science and Engineering grant to P. Kelemen and J. Matter; the Arthur D. Storke Chair at Columbia University, NSF-MGG-1059175, and NSF-EAR-1049905 to P. Kelemen.

APPENDIX A. ESTIMATION OF THE OXYGEN ISOTOPE AND CLUMPED ISOTOPE COMPOSITION OF HCO_3^- DERIVED FROM CO_2 HYDROXYLATION REACTION

The CO_2 hydroxylation reaction is ubiquitous in aqueous solutions containing dissolved inorganic carbon:

$$CO_2 + OH^- \rightarrow HCO_3^-$$

In high pH solutions, CO_2 hydroxylation is the dominant reaction path by which CO_2 converts to HCO_3^- (Pinsent et al., 1956). To obtain a first order estimation on the oxygen isotope and clumped isotope composition of the HCO_3^- derived from CO_2 hydroxylation, we assume (1) there is no kinetic isotope fractionation associated with CO_2 hydroxylation, i.e. the addition of OH^- is random, and (2) the isotopic compositions of both CO_2 and OH^- are in equilibrium with water at assumed temperatures (Clark et al., 1992; Rollion-Bard et al., 2003). We then calculate the abundances of different HCO_3^- isotopologues, by considering the reactions between all 12 stable isotopologues of CO_2 and 3 oxygen isotopologues of OH^-:

$$^{12}C^{16}O^{16}O + {}^{16}OH^- \rightarrow H^{12}C^{16}O^{16}O^{16}O^-$$
$$^{12}C^{16}O^{16}O + {}^{17}OH^- \rightarrow H^{12}C^{17}O^{16}O^{16}O^-$$
$$^{12}C^{16}O^{16}O + {}^{18}OH^- \rightarrow H^{12}C^{18}O^{16}O^{16}O^-$$
$$\ldots\ldots$$
$$^{13}C^{16}O^{16}O + {}^{16}OH^- \rightarrow H^{13}C^{16}O^{16}O^{16}O^-$$
$$^{13}C^{16}O^{16}O + {}^{17}OH^- \rightarrow H^{13}C^{17}O^{16}O^{16}O^-$$
$$^{13}C^{16}O^{16}O + {}^{18}OH^- \rightarrow H^{13}C^{18}O^{16}O^{16}O^-$$
$$\ldots\ldots$$

The abundances of different CO2 isotopologues at assumed temperatures are calculated following the methodology and algorithms described by Wang et al. (2004).

At 300 K, for $\delta^{13}C_{CO2,\ VPDB} = 0‰$ and $\delta^{18}O_{water,\ VSMOW} = 0‰$, our calculation yields $\delta^{18}O_{CO2,\ VSMOW} = 41.6‰$, $\delta^{18}O_{OH-,\ VSMOW} = -37.6‰$ and $\Delta_{47,\ CO2} = 0.924‰$ (Brenninkmeijer et al., 1983; Green and Taube, 1963; Wang et al., 2004). Accordingly, the isotopic composition of the HCO_3^- derived from CO_2 hydroxylation reaction is estimated to be $\delta^{13}C_{HCO3-,\ VPDB} = 0‰$, $\delta^{18}O_{HCO3-,\ VSMOW} = 15.2‰$, and $\Delta_{63} = 0.590‰$, where Δ_{63} denotes the extent of ^{13}C-^{18}O clumping (mostly) in the HCO_3^- and is defined the same way as in Guo et al. (2009). This estimated isotope composition of HCO_3^- is depleted in $\delta^{18}O$ but enriched in Δ_{63}, compared to the expected equilibrium isotope composition of HCO_3^- at 300 K (i.e., $\delta^{18}O_{HCO3-,\ VSMOW} = 31.1‰$, $\Delta_{63} = 0.397‰$; Beck et al., 2005; Hill et al., 2014), with an apparent Δ_{63}-$\delta^{18}O$ slope of −0.012. In high pH solutions, CO_3^{2-} comprises a far greater proportion of the DIC pool than HCO_3^-, but isotopic equilibration between HCO_3^- and CO_3^{2-} is effectively instantaneous, with an equilibrium Δ_{63} fractionation of 0.033–0.063‰ (Tripati et al., 2015). Therefore, the magnitude of clumped isotope enrichment and ^{18}O depletion in the total DIC pool will be inherited from the HCO_3^- formed during the hydroxylation reaction. This is expected to lead to an apparent Δ_{47}-$\delta^{18}O$ slope of the same magnitude in the carbonate solids derived from CO_2 hydroxylation reaction (Section 5.1.1, Guo et al., 2009).

APPENDIX B. EFFECTS OF CARBONATE MIXING ON APPARENT ^{14}C AGES OF TRAVERTINE

Precipitation of later generations of carbonates within the pore space of the travertine (e.g. in preserved travertine terrace OM10-32C), if unaccounted for, can result in significant errors in estimating the true formation ages of travertine samples based on ^{14}C method (Section 5.2.2). To illustrate this, we calculate possible ranges of "true" ages for the initial formation of travertine OM10-32C subsamples.

We assume that the precipitation of "contaminant" carbonate within the travertine pore space occurred at the same time for all sub-samples and did not incorporate any dead carbon. Under these assumptions, the fraction modern carbon (Fm) of the hypothetical contaminant

Table B.1
Calculated "true" ages of travertine subsamples.

Sample	Type	% Secondary end-member	Measured ^{14}C		Max. contaminant Fm		Min. contaminant Fm	
Sample Name			Fm	^{14}C age	"True" Fm	^{14}C age	"True" Fm	^{14}C age
Hypothetical	Contaminating end-member	100			0.462	7100	0.369	8890
OM10-32C-11	Mixed travertine	78.0	0.369	8890	0.040	30140	0.369	8890
OM10-32C-10	Mixed travertine	42.8	0.198	15640	0.000	>50000	0.069	25760
OM10-32C-8	Mixed travertine	8.2	0.153	18350	0.125	20160	0.133	19550
OM10-32C-9	Travertine end-member	0	0.031	32010				

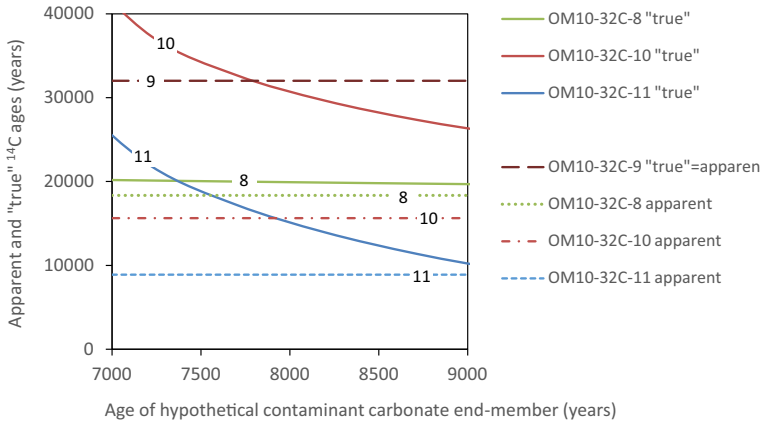

Fig. B.1. Calculated "true" ages of travertine subsamples of nOM10-32C versus the assumed age of the hypothetical contaminant carbonate end-member (e.g., later generations of carbonate precipitated within travertine pore space). "Apparent" (measured) ^{14}C ages (dotted or dashed lines) are plotted for comparison with the calculated "true" ages (solid lines). The proportions of contaminant carbonate end-member used in the calculation of "true" ages are as calculated in Section 5.2.2 and shown in Fig. 7: 8% in OM10-32C-8, 0% in OM10-32C-9, 43% in OM10-32C-10, and 78% OM10-32C-11. Subsamples with significant proportions of the contaminant carbonate end-member may have "true" ages tens of thousands of years older than the apparent ^{14}C ages (e.g., OM10-32C-10 and OM10-32C-11). The apparent relative chronology of the travertine subsamples can also be substantially changed by mixing with later generations of carbonate. For example, the measured apparent ^{14}C ages suggest OM10-32C-9 is the oldest, followed by sample OM10-32C-8, OM10-32C-10, then OM10-32C-11, but depending on the age of the contaminating end-member, the "true" order of these OM10-32C subsamples could be 10, 9, 11, 8; 10, 9, 8, 11; or 9, 10, 8, 11.

end-member is constrained by the maximum measured Fm in the travertine subsamples and the minimum possible "true" Fm. In other words, the hypothetical contaminant end-member cannot be older than the most recent travertine subsample, and it cannot be so young that the calculated "true" Fm would be less than zero for any subsample. We then calculate the "true" Fm and corresponding ^{14}C age of each subsample that would produce their measured apparent ages, using the proportions of hypothetical contaminant carbonates estimated in Section 5.2.2 and shown in Fig. 7.

Depending on the assumed value for the Fm of the contaminant end-member, the calculated "true" ages of the travertine can be tens of thousands of years older than their apparent ^{14}C ages and even relative order of formation for the subsamples can change (Table B.1, Fig. B.1). Note, in reality, the contaminant carbonates could have formed over multiple episodes or could have incorporated dead carbon. Therefore, the true ages of the travertine can be even less well-constrained.

APPENDIX C. SUPPLEMENTARY DATA

Supplementary data associated with this article can be found, in the online version, at http://dx.doi.org/10.1016/j.gca.2016.06.026.

REFERENCES

Affek H. P. (2012) Clumped isotope paleothermometry: Principles, applications, and challenges. In *Reconstructing Earth's Deep-Time Climate – The State of the Art in 2012* (eds. L. C. Ivany and B. Huber). Paleontological Society Papers, pp. 101–114.

Affek H. P. and Eiler J. M. (2006) Abundance of mass 47 CO2 in urban air, car exhaust, and human breath. *Geochim. Cosmochim. Acta* **70**, 1–12.

Affek H. P., Bar-Matthews M., Ayalon A., Matthews A. and Eiler J. M. (2008) Glacial/interglacial temperature variations in Soreq cave speleothems as recorded by 'clumped isotope' thermometry. *Geochim. Cosmochim. Acta* **72**, 5351–5360.

Affek H. P., Matthews A., Ayalon A., Bar-Matthews M., Burstyn Y., Zaarur S. and Zilberman T. (2014) Accounting for kinetic

isotope effects in Soreq Cave (Israel) speleothems. *Geochim. Cosmochim. Acta* **143**, 303–318.

Barnes I. and O'Neil J. R. (1969) Relationship between fluids in some fresh alpine-type ultramafics and possible modern serpentinization, western United States. *GSA Bull.* **80**, 1947–1960.

Barnes I., LaMarche V. C. and Himmelberg G. (1967) Geochemical evidence of present-day serpentinization. *Science* **156**, 830–832.

Barnes I., O'Neil J. R. and Trescases J. J. (1978) Present day serpentinization in new-caledonia, Oman and Yugoslavia. *Geochim. Cosmochim. Acta* **42**, 144–145.

Beck W. C., Grossman E. L. and Morse J. W. (2005) Experimental studies of oxygen isotope fractionation in the carbonic acid system at 15° 25° and 40°C. *Geochim. Cosmochim. Acta* **69**, 3493–3503.

Boudier F. and Coleman R. G. (1981) Cross section through the peridotite in the Semail ophiolite. *J. Geophys. Res.* **86**, 2573–2592.

Boudier F., Baronnet A. and Mainprice D. (2010) Serpentine mineral replacements of natural olivine and their seismic implications: Oceanic lizardite versus subduction-related antigorite. *J. Petrol.* **51**, 495–512.

Brenninkmeijer C. A. M., Kraft P. and Mook W. G. (1983) Oxygen isotope fractionation between CO_2 and H_2O. *Isot. Geosci.* **1**, 181–190.

Bruni J., Canepa M., Chiodini G., Cioni R., Cipolli F., Longinelli A., Marini L., Ottonello G. and Zuccolini M. V. (2002) Irreversible water-rock mass transfer accompanying the generation of the neutral, Mg-HCO3 and high-pH, Ca-OH spring waters of the Genova province, Italy. *Appl. Geochem.* **17**, 455–474.

Burns S. J. and Matter A. (1995) Geochemistry of carbonate cements in surficial alluvial conglomerates and their paleoclimatic implications, Sultanate-of-Oman. *J. Sediment. Res. A* **65**, 170–177.

Burns S. J., Fleitmann D., Matter A., Neff U. and Mangini A. (2001) Speleothem evidence from Oman for continental pluvial events during interglacial periods. *Geology* **29**, 623–626.

Came R. E., Brand U. and Affek H. P. (2014) Clumped isotope signatures in modern brachiopod carbonate. *Chem. Geol.* **377**, 20–30. http://dx.doi.org/10.1016/j.chemgeo.2014.04.004.

Cardace D., Meyer-Dombard D. A. R., Woycheese K. and Arcilla C. A. (2015) Feasible metabolic schema associated with high pH springs in the Philippines. *Front. Microbiol.* **6**.

Chavagnac V., Ceuleneer G., Monnin C., Lansac B., Hoareau G. and Boulart C. (2013a) Mineralogical assemblages forming at hyperalkaline warm springs hosted on ultramafic rocks: A case study of Oman and Ligurian ophiolites. *Geochem. Geophys. Geosys.* **14**, 2474–2495.

Chavagnac V., Monnin C., Ceuleneer G., Boulart C. and Hoareau G. (2013b) Characterization of hyperalkaline fluids produced by low-temperature serpentinization of mantle peridotites in the Oman and Ligurian ophiolites. *Geochem. Geophys. Geosys.* **14**, 2496–2522.

Cipolli F., Gambardella B., Marini L., Ottonello G. and Zuccolini M. V. (2004) Geochemistry of high-pH waters from serpentinites of the Gruppo di Voltri (Genova, Italy) and reaction path modeling of CO2 sequestration in serpentinite aquifers. *Appl. Geochem.* **19**, 787–802.

Clark I. D. and Fontes J. C. (1990) Paleoclimatic reconstruction in northern Oman based on carbonates from hyperalkaline groundwaters. *Quat. Res.* **33**, 320–336.

Clark I. D., Fontes J. C. and Fritz P. (1992) Stable isotope disequilibria in travterine from high pH-waters – Laboratory investigations and field observations from Oman. *Geochim. Cosmochim. Acta* **56**, 2041–2050.

Craig H. (1961) Isotopic variations in meteoric waters. *Science* **133**, 1702–1703.

Daeron M., Guo W., Eiler J., Genty D., Blamart D., Boch R., Drysdale R., Maire R., Wainer K. and Zanchetta G. (2011) (CO)-C-13-O-18 clumping in speleothems: Observations from natural caves and precipitation experiments. *Geochim. Cosmochim. Acta* **75**, 3303–3317.

Defliese W. F., Hren M. T. and Lohmann K. C. (2015) Compositional and temperature effects of phosphoric acid fractionation on Δ47 analysis and implications for discrepant calibrations. *Chem. Geol.* **396**, 51–60.

Defliese W. F. and Lohmann K. C. (2015) Non-linear mixing effects on mass-47 CO2 clumped isotope thermometry: Patterns and implications. *Rapid Commun. Mass Spectrom.* **29**, 901–909.

Dennis K. J. and Schrag D. P. (2010) Clumped isotope thermometry of carbonatites as an indicator of diagenetic alteration. *Geochim. Cosmochim. Acta* **74**, 4110–4122.

Dennis K. J., Affek H. P., Passey B. H., Schrag D. P. and Eiler J. M. (2011) Defining an absolute reference frame for 'clumped' isotope studies of CO2. *Geochim. Cosmochim. Acta* **75**, 7117–7131.

Dietzel M., Usdowski E. and Hoefs J. (1992) Chemical and C-13/C-12-isotope and O-18/O-16-isotope evolution of alkaline drainage waters and the precipitation of calcite. *Appl. Geochem.* **7**, 177–184.

Eagle R. A., Eiler J. M., Tripati A. K., Ries J. B., Freitas P. S., Hiebenthal C., Wanamaker A. D., Taviani M., Elliot M., Marenssi S., Nakamura K., Ramirez P. and Roy K. (2013) The influence of temperature and seawater carbonate saturation state on ^{13}C–^{18}O bond ordering in bivalve mollusks. *Biogeosciences* **10**, 4591–4606.

Ehlmann B. L., Mustard J. F. and Murchie S. L. (2010) Geologic setting of serpentine deposits on Mars. *Geophys. Res. Lett.* **37**.

Eiler J. (2007) "Clumped-isotope" geochemistry: The study of naturally occurring, multiply-substituted isotopologues. *Earth Planet. Sci. Lett.* **262**, 309–327.

Eiler J. M. (2011) Paleoclimate reconstruction using carbonate clumped isotope thermometry. *Quat. Sci. Rev.* **30**, 3575–3588.

Eiler J. M. and Schauble E. (2004) (OCO)-O-18-C-13-O-16 in Earth's atmosphere. *Geochim. Cosmochim. Acta* **68**, 4767–4777.

Epstein S. and Mayeda T. (1953) Variation of O18 content of waters from natural sources. *Geochim. Cosmochim. Acta* **4**, 213–224.

Etiope G., Ehlmann B. L. and Schoell M. (2013) Low temperature production and exhalation of methane from serpentinized rocks on Earth: A potential analog for methane production on Mars. *Icarus* **224**, 276–285.

Falk E. S. (2013) *Carbonation of Peridotite in the Oman Ophiolite* (Ph.D. thesis). Columbia University.

Falk E. S. and Kelemen P. B. (2015) Geochemistry and petrology of listvenite in the Samail ophiolite, Sultanate of Oman: Complete carbonation of peridotite during ophiolite emplacement. *Geochim. Cosmochim. Acta* **160**, 70–90.

Fleitmann D., Burns S. J., Neff U., Mangini A. and Matter A. (2003) Changing moisture sources over the last 330,000 years in Northern Oman from fluid-inclusion evidence in speleothems. *Quat. Res.* **60**, 223–232.

Gehre M., Hoefling R., Kowski P. and Strauch G. (1996) Sample preparation device for quantitative hydrogen iso-tope analysis using chromium metal. *Anal. Chem.* **68**, 4414–4417.

Ghosh P., Adkins J., Affek H., Balta B., Guo W., Schauble E. A., Schrag D. and Eiler J. M. (2006) 13C–18O bonds in carbonate minerals: A new kind of paleothermometer. *Geochim. Cosmochim. Acta* **70**, 1439–1456.

Godard M., Jousselin D. and Bodinier J.-L. (2000) Relationships between geochemistry and structure beneath a palaeo-spreading centre: a study of the mantle section in the Oman ophiolite. *Earth Planet. Sci. Lett.* **180**, 133–148.

Guo W. (2008) *Carbonate Clumped Isotope Thermometry: Application to Carbonaceous Chondrites and Effects of Kinetic Isotope Fractionation* (Ph.D. thesis). California Institute of Technology.

Guo W. F., Mosenfelder J. L., Goddard W. A. and Eiler J. M. (2009) Isotopic fractionations associated with phosphoric acid digestion of carbonate minerals: Insights from first-principles theoretical modeling and clumped isotope measurements. *Geochim. Cosmochim. Acta* **73**, 7203–7225.

Grauel A.-L., Schmid T. W., Hu B., Bergami C., Capotondi L., Zhou L. and Bernasconi S. M. (2013) Calibration and application of the 'clumped isotope' thermometer to foraminifera for high-resolution climate reconstructions. *Geochim. Cosmochim. Acta* **108**, 125–140.

Green M. and Taube H. (1963) Isotopic fractionation in the OH–H2O exchange reaction. *J. Phys. Chem.* **67**, 1565–1566.

Halevy I., Fischer W. W. and Eiler J. M. (2011) Carbonates in the Martian meteorite Allan Hills 84001 formed at 18 +/- 4 degrees C in a near-surface aqueous environment. *Proc. Natl. Acad. Sci. U.S.A.* **108**, 16895–16899.

Hanghøj K., Kelemen P. B., Hassler D. and Godard M. (2010) Composition and genesis of depleted mantle peridotites from the Wadi Tayin massif, Oman ophiolite: Major and trace element geochemistry, and Os isotope and PGE systematics. *J. Petrol.* **51**, 206–227.

Henkes G. A., Passey B. H., Wanamaker, Jr., A. D., Grossman E. L., Ambrose, Jr., W. G. and Carroll M. L. (2013) Carbonate clumped isotope compositions of modern marine mollusk and brachiopod shells. *Geochim. Cosmochim. Acta* **106**, 307–325.

Hill P. S., Tripati A. K. and Schauble E. A. (2014) Theoretical constraints on the effects of pH, salinity, and temperature on clumped isotope signatures of dissolved inorganic carbon species and precipitating carbonate minerals. *Geochim. Cosmochim. Acta* **125**, 610–652.

Huntington K. W. and Lechler A. R. (2015) Carbonate clumped isotope thermometry in continental tectonics. *Tectonophysics* **647–648**, 1–20.

Huntington K. W., Eiler J. M., Affek H. P., Guo W., Bonifacie M., Yeung L. Y., Thiagarajan N., Passey B., Tripati A., Daëron M. and Came R. (2009) Methods and limitations of 'clumped' CO_2 isotope (Δ47) analysis by gas-source isotope ratio mass spectrometry. *J. Mass Spectrom.* **44**, 1318–1329.

Kele S., Breitenbach S. F., Capezzuoli E., Meckler A. N., Ziegler M., Millan I. M., Kluge T., Deák J., Hanselmann K., John C. M. and Yan H. (2015) Temperature dependence of oxygen-and clumped isotope fractionation in carbonates: A study of travertines and tufas in the 6–95 C temperature range. *Geochim. Cosmochim. Acta* **168**, 172–192.

Kelemen P. B. and Matter J. (2008) In situ carbonation of peridotite for CO2 storage. *Proc. Natl. Acad. Sci. U.S.A.* **105**, 17295–17300.

Kelemen P. B., Matter J., Streit E. E., Rudge J. F., Curry W. B. and Bluztajn J. (2011) Rates and mechanisms of mineral carbonation in peridotite: Natural processes and recipes for enhanced, in situ CO_2 capture and storage. *Ann. Rev. Earth Planet. Sci.* **39**, 545–576.

Kim S. T. and O'Neil J. R. (1997) Equilibrium and nonequilibrium oxygen isotope effects in synthetic carbonates. *Geochim. Cosmochim. Acta* **61**, 3461–3475.

Kim S. T., O'Neil J. R., Hillaire-Marcel C. and Mucci A. (2007) Oxygen isotope fractionation between synthetic aragonite and water: influence of temperature and Mg 2+ concentration. *Geochim. Cosmochim. Acta* **71**, 4704–4715.

Kluge T. and Affek H. P. (2012) Quantifying kinetic fractionation in Bunker Cave speleothems using Δ47. *Quat. Sci. Rev.* **49**, 82–94.

Kluge T., Affek H. P., Zhang Y. G., Dublyansky Y., Spötl C., Immenhauser A. and Richter D. K. (2014) Clumped isotope thermometry of cryogenic cave carbonates. *Geochim. Cosmochim. Acta* **126**, 541–554.

Kluge T., John C. M., Jourdan A.-L., Davis S. and Crawshaw J. (2015) Laboratory calibration of the calcium carbonate clumped isotope thermometer in the 25–250;°C temperature range. *Geochim. Cosmochim. Acta* **157**, 213–227.

Kosednar-Legenstein B., Dietzel M., Leis A. and Stingl K. (2008) Stable carbon and oxygen isotope investigation in historical lime mortar and plaster – Results from field and experimental study. *Appl. Geochem.* **23**, 2425–2437.

Marques J. M., Carreira P. M., Carvalho M. R., Matias M. J., Goff F. E., Basto M. J., Graça R. C., Aires-Barros L. and Rocha L. (2008) Origins of high pH mineral waters from ultramafic rocks, Central Portugal. *Appl. Geochem.* **23**, 3278–3289.

Matter J. M. (2005) Recharge areas and geochemical evolution of groundwater in an alluvial aquifer system in the Sultanate of Oman. *Hydrogeol. J.* **14**, 203–224.

Matter J. M. and Kelemen P. B. (2009) Permanent CO2 storage and mineral carbonation in geologic reservoirs. *Nat. Geosci.* **2**, 837–841.

McCrea J. M. (1950) On the isotopic chemistry of carbonates and a paleotemperature scale. *J. Chem. Phys.* **18**, 849–857.

Mervine E. M., Humphris S. E., Sims K. W. W., Kelemen P. B. and Jenkins W. J. (2014) Carbonation rates of peridotite in the Samail Ophiolite, Sultanate of Oman, constrained through 14C dating and stable isotopes. *Geochim. Cosmochim. Acta* **126**, 371–397.

Mervine E. M., Sims K. W. W., Humphris S. E. and Kelemen P. B. (2015) Applications and limitations of U-Th disequilibria systematics for determining ages of carbonate alteration minerals in peridotite. *Chem. Geol.* **412**, 151–166.

Monnier C., Girardeau J., Le Mée L. and Polvé M. (2006) Along-ridge petrological segmentation of the mantle in the Oman ophiolite. *Geochem. Geophys. Geosys.* **7**.

Neal C. and Stanger G. (1983) Hydrogen generation from mantle source rocks in Oman. *Earth Planet. Sci. Lett.* **66**, 315–320.

Neal C. and Stanger G. (1985) Past and present serpentinization of ultramafic rocks: An example from the Semail ophiolite nappe of northern Oman. In *The Chemistry of Weathering* (ed. J. I. Drewer). D. Reidel Publishing Company, Holland, pp. 249–275.

Neal C. and Shand P. (2002) Spring and surface water quality of the Cyprus ophiolites. *Hydrol. Earth Syst. Sci.* **6**, 797–817.

Niles P. B., Leshin L. A. and Guan Y. (2005) Microscale carbon isotope variability in ALH84001 carbonates and a discussion of possible formation environments. *Geochim. Cosmochim. Acta* **69**, 2931–2944.

Niles P., Catling D., Berger G., Chassefière E., Ehlmann B., Michalski J., Morris R., Ruff S. and Sutter B. (2013) Geochemistry of Carbonates on Mars: Implications for Climate History and Nature of Aqueous Environments. *Space Sci. Rev.* **174**, 301–328.

Olsson I. U. (1970) The use of oxalic acid as a standard. In *Radiocarbon Variations and Absolute Chronology, Nobel Symposium, 12th Proc.* John Wiley and Sons, New York, p. 17.

Oman Directorate General of Meteorology (2015) Nizwa historical climate data, 1986–2009. http://www.met.gov.om/opencms/export/sites/default/dgman/en/weather-chart/historical-data/.

O'Neil J. R. and Barnes I. (1971) C13 and O18 compositions in some fresh-water carbonates associated with ultramafic rocks and serpentinites: western United States. *Geochim. Cosmochim. Acta* **35**, 687–697.

Oze C. and Sharma M. (2005) Have olivine, will gas: Serpentinization and the abiogenic production of methane on Mars. *Geophys. Res. Lett.* **32**, L10203.

Paukert A. N., Matter J. M., Kelemen P. B., Shock E. L. and Havig J. R. (2012) Reaction path modeling of enhanced in situ

CO2 mineralization for carbon sequestration in the peridotite of the Samail Ophiolite, Sultanate of Oman. *Chem. Geol.* **330–331**, 86–100.

Pinsent B. R. W., Pearson L. and Roughton F. J. W. (1956) The kinetics of combination of carbon dioxide with hydroxide ions. *Trans. Faraday Soc.* **52**, 2930–2934.

Reimer P., Bard E., Bayliss A., Beck J., Blackwell P., Bronk Ramsey C., Buck C., Cheng H., Edwards R., Friedrich M., Grootes P., Guilderson T., Haflidason H., Hajdas I., Hatté C., Heaton T., Hoffmann D., Hogg A., Hughen K., Kaiser K., Kromer B., Manning S., Niu M., Reimer R., Richards D., Scott E., Southon J., Staff R., Turney C. and van der Plicht J. (2013) IntCal13 and Marine13 radiocarbon age calibration curves 0–50,000 years cal BP. *Radiocarbon* **55**(4), 1869–1887.

Rollion-Bard C., Chaussidon M. and France-Lanord C. (2003) PH control on oxygen isotopic composition of symbiotic corals. *Earth Planet. Sci. Lett.* **215**, 275–288.

Saenger C., Affek H. P., Felis T., Thiagarajan N., Lough J. M. and Holcomb M. (2012) Carbonate clumped isotope variability in shallow water corals: Temperature dependence and growth-related vital effects. *Geochim. Cosmochim. Acta* **99**, 224–242.

Schmid T. W. (2011) *Clumped Isotopes: A New Tool for Old Questions* (Ph.D. thesis). Eidgenössische Technische Hochschule ETH Zürich.

Spooner P. T., Guo W., Robinson L. F., Thiagarajan N., Hendry K., Rosenheim B. E. and Leng M. J. (2016) Clumped isotope composition of cold-water corals: A role for vital effects? *Geochim. Cosmochim. Acta* **179**, 123–141.

Streit E., Kelemen P. and Eiler J. (2012) Coexisting serpentine and quartz from carbonate-bearing serpentinized peridotite in the Samail Ophiolite, Oman. *Contrib. Mineral. Petrol.* **164**, 821–837.

Szponar N., Brazelton W. J., Schrenk M. O., Bower D. M., Steele A. and Morrill P. L. (2013) Geochemistry of a continental site of serpentinization, the Tablelands Ophiolite, Gros Morne National Park: A Mars analogue. *Icarus* **224**, 286–296.

Tang J., Dietzel M., Fernandez A., Tripati A. K. and Rosenheim B. E. (2014) Evaluation of kinetic effects on clumped isotope fractionation (Δ47) during inorganic calcite precipitation. *Geochim. Cosmochim. Acta* **134**, 120–136.

Thiagarajan N., Adkins J. and Eiler J. (2011) Carbonate clumped isotope thermometry of deep-sea corals and implications for vital effects. *Geochim. Cosmochim. Acta* **75**, 4416–4425.

Thornalley D. J. R., Bauch H. A., Gebbie G., Guo W., Ziegler M., Bernasconi S. M., Barker S., Skinner L. C. and Yu J. (2015) A warm and poorly ventilated deep Arctic Mediterranean during the last glacial period. *Science* **349**, 706–710.

Tripati A. K., Eagle R. A., Thiagarajan N., Gagnon A. C., Bauch H., Halloran P. R. and Eiler J. M. (2010) C-13-O-18 isotope signatures and 'clumped isotope' thermometry in foraminifera and coccoliths. *Geochim. Cosmochim. Acta* **74**, 5697–5717.

Tripati A. K., Hill P. S., Eagle R. A., Mosenfelder J. L., Tang J., Schauble E. A., Eiler J. M., Zeebe R. E., Uchikawa J., Coplen T. B., Ries J. B. and Henry D. (2015) Beyond temperature: Clumped isotope signatures in dissolved inorganic carbon species and the influence of solution chemistry on carbonate mineral composition. *Geochim. Cosmochim. Acta* **166**, 344–371.

Wainer K., Genty D., Blamart D., Daëron M., Bar-Matthews M., Vonhof H., Dublyansky Y., Pons-Branchu E., Thomas L., van Calsteren P., Quinif Y. and Caillon N. (2011) Speleothem record of the last 180 ka in Villars cave (SW France): Investigation of a large δ18O shift between MIS6 and MIS5. *Quat. Sci. Rev.* **30**, 130–146.

Wang Z. G., Schauble E. A. and Eiler J. M. (2004) Equilibrium thermodynamics of multiply substituted isotopologues of molecular gases. *Geochim. Cosmochim. Acta* **68**, 4779–4797.

Weyhenmeyer C. E., Burns S. J., Waber H. N., Aeschbach-Hertig W., Kipfer R., Loosli H. H. and Matter A. (2000) Cool glacial temperatures and changes in moisture source recorded in Oman groundwaters. *Science* **287**, 842–845.

Wilson S. A., Dipple G. M., Power I. M., Thom J. M., Anderson R. G., Raudsepp M., Gabities J. E. and Southam G. (2009) Carbon dioxide fixation within mine wastes of ultramafic-hosted ore deposits: Examples from the Clinton Creek and Cassiar Chrysotile deposits, Canada. *Econ. Geol.* **104**, 95–112.

Wilson S. A., Barker S. L. L., Dipple G. M. and Atudorei V. (2010) Isotopic Disequilibrium during Uptake of Atmospheric CO_2 into Mine Process Waters: Implications for CO2 Sequestration. *Environ. Sci. Technol.* **44**, 9522–9529.

Zaarur S., Affek H. P. and Brandon M. (2013) A revised calibration of the clumped isotope thermometer. *Earth Planet. Sci. Lett.* **382**, 47–57.

Zeebe R. E. and Wolf-Gladrow D. A. (2001) *CO_2 in Seawater: Equilibrium, Kinetics, Isotopes*. Elsevier, Amsterdam.

Associate editor: Miryam Bar-Matthews